

## Experimental investigation of soil–structure interface behaviour under monotonic and cyclic thermal loading

Guo, Yimu; Golchin, Ali; Hicks, Michael A.; Liu, Songyu; Zhang, Guozhu; Vardon, Philip J.

**DOI**

[10.1007/s11440-022-01781-5](https://doi.org/10.1007/s11440-022-01781-5)

**Publication date**

2023

**Document Version**

Final published version

**Published in**

Acta Geotechnica

**Citation (APA)**

Guo, Y., Golchin, A., Hicks, M. A., Liu, S., Zhang, G., & Vardon, P. J. (2023). Experimental investigation of soil–structure interface behaviour under monotonic and cyclic thermal loading. *Acta Geotechnica*, 18(7), 3585-3608. <https://doi.org/10.1007/s11440-022-01781-5>

**Important note**

To cite this publication, please use the final published version (if applicable). Please check the document version above.

**Copyright**

Other than for strictly personal use, it is not permitted to download, forward or distribute the text or part of it, without the consent of the author(s) and/or copyright holder(s), unless the work is under an open content license such as Creative Commons.

**Takedown policy**

Please contact us and provide details if you believe this document breaches copyrights. We will remove access to the work immediately and investigate your claim.



# Experimental investigation of soil–structure interface behaviour under monotonic and cyclic thermal loading

Yimu Guo<sup>1,2</sup> · Ali Golchin<sup>2</sup> · Michael A. Hicks<sup>2</sup> · Songyu Liu<sup>1</sup> · Guozhu Zhang<sup>1</sup> · Philip J. Vardon<sup>2</sup>

Received: 6 July 2022 / Accepted: 14 December 2022  
© The Author(s) 2023

## Abstract

The effect of temperature on the monotonic and cyclic shearing response of a soil–structure interface is of critical importance for the application of thermal-active geo-structures. To investigate this, soils and soil–concrete interfaces were comprehensively tested with a temperature-controlled direct shear device under both fixed temperatures and thermal/mechanical cycles within the range of 2–38 °C. Monotonic and cyclic shearing with various boundary conditions, including constant normal load (CNL), constant normal stiffness (CNS) and constant volume (CV), were conducted to resemble the conditions that thermal-active-geo-structures may experience. The strength properties of the sand, clay, and sand–concrete and clay–concrete interfaces were partially influenced by heating and cooling under all boundary conditions. However, several effects were observed which could affect the performance of thermo-active structures. Heating cycles caused the clay–concrete interface to be overconsolidated, implying a lower excess pore pressure would be generated during shearing. The cyclic CNS tests suggested that the interface strength could degrade due to (thermally induced) cyclic shear displacements, with this effect strongly related to the state of the soil rather than the temperature directly. In these tests, the medium-dense sand–concrete interface degraded to almost zero shear strength after 5 cycles, whereas the clay–concrete interface asymptotically degraded to around 60% of its strength after 10 cycles.

**Keywords** Laboratory test · Shear strength · Soil–structure interaction · Temperature effects

## 1 Introduction

Thermo-active geo-structures have been shown to have the potential to efficiently harvest shallow geothermal energy. At depths below 5–7 m, the temperature of the ground is relatively stable, which allows the ground to be reliable and efficient as a heat source in the winter and a heat sink in the summer [1]. The soils adjacent to the structure are typically subjected to annual and daily cyclic temperature variation, depending on the operation mode of the ground source heat pump (GSHP) system. The mechanical behaviour of the soil and soil–structure interaction may change due to these thermal effects and thereby influence the bearing capacity

or settlement of the structure. At the same time, the thermally induced deformation of the structure was found to impose cyclic shearing along the interface [2, 3], which may also impact the bearing capacity or settlements. The thermo-mechanical behaviour of soils has been investigated thoroughly under triaxial boundary conditions [4–12], while investigations on thermo-mechanical response at the interface level have just begun [13]. Therefore, a more comprehensive investigation into the thermo-mechanical behaviour of interfaces subjected to monotonic and cyclic thermal loadings, as well as on thermal effects on the cyclic shearing induced by energy structures, is required.

The isothermal behaviour of a soil–structure interface element depends on several factors, such as the material type (wood, steel or concrete) of the structure [14], the surface roughness [15–18], soil crushability [19], particle angularity [20–22], particle size [23], the rate of shearing [24], and soil anisotropy [25]. Amongst these, the soil mean particle size and the roughness of the surface of the

✉ Philip J. Vardon  
P.J.Vardon@tudelft.nl

<sup>1</sup> Institute of Geotechnical Engineering, Southeast University, Nanjing, Jiangsu, People's Republic of China

<sup>2</sup> Faculty of Civil Engineering and Geosciences, Delft University of Technology, 2600 GA Delft, Netherlands

structure play a crucial role, for which the normalised roughness  $R_n$  was proposed [16, 26]:

$$R_n = \frac{R_{\max}(L = D_{50})}{D_{50}} \quad (1)$$

where  $R_{\max}$  is the distance between the highest peak and lowest valley within a gauged length of  $L = D_{50}$  (where  $D_{50}$  is the mean particle size).  $R_n$  is suitable for describing granular material interfaces because it considers the microscopic angle between asperities and the particles, while parameter  $R_{\max}$  is more often used to characterise clay interfaces, due to the difference in failure mechanism along the interface (i.e. sliding of a thin layer of oriented clay) [27, 28]. The roughness was shown to be linearly correlated with the soil interface friction coefficient before prior to a threshold value, after which the friction coefficient approached that of the soil indicating a failure inside the soil rather than along the soil–structure interface [19, 24, 29].

Another aspect influencing the mechanical response of the soil interface is the boundary conditions. The volumetric response of the shear zone (a thin layer around structures where large shear strains are localised) during shearing can alter the normal stress applied to the interface (depending on the normal boundary conditions) which could lead to a different shear resistance. The boundary conditions may be categorised into constant normal load (CNL), constant normal stiffness (CNS), and constant volume (CV) using the normal stiffness ( $K$ ) [30]:

$$K = \frac{\Delta\sigma}{\Delta\delta} \quad (2)$$

where  $\Delta\sigma$  is the normal stress variation, and  $\Delta\delta$  is the normal displacement variation on the interface. In a conventional direct shear test, samples are sheared with the CNL condition ( $K = 0$ , Fig. 1a), which is the simplest way to determine the shear strength parameters [26]. In some applications, deformations in the shear zone are confined by the surrounding soil, which leads to changes in the normal stress. In these applications, the shear resistance could be more rationally determined under the CNS

condition ( $K = \text{constant}$ , Fig. 1b) [31]. This was verified by comparing centrifuge, in situ pile experiments and laboratory CNS tests [32–34]. Cyclic degradation of the pile interface was successfully replicated by cyclic CNS tests [35, 36]. In some direct shear tests, the height of the specimen during shearing may be fixed (also known as constant volume, i.e. CV). For these tests, the normal stiffness tends to infinity ( $K = \infty$ , Fig. 1c) and represents an equivalent undrained shear condition [27, 37, 38]. The vertical stress change in CV shearing is equal to the pore pressure developed during undrained direct shear tests [39].

During energy pile system operations, these boundary conditions may be encountered along the soil–structure interface in different circumstances. For GSHP systems operating continuously, the temperature at the interface is expected to change monotonically until a quasi-static heat transfer is reached. Since the temperature is almost unchanged or varies at a relatively low rate, the normal stress on the structure is expected to be relatively constant (e.g. thermal expansion of structure, volume change of the interface induced by soil–structure displacement is negligible) resembling the CNL condition. For intermittent operation, where the energy pile provides both heating and cooling at different periods during the year and/or only operates for given hours within a day, the thermal impulse could cause significant short-term temperature fluctuations. The cyclic shearing imposed by thermal deformation of the pile is more likely to be confined elastically by the surrounding soil, resembling the CNS condition. For energy piles bearing a variable load (e.g. in a de-icing system for a bridge deck [40]) or for short-term thermal loads, the loading would impose a “fast shearing” along the soil–structure interface, which can be undrained and can be investigated under CV conditions. Therefore, it is of interest to evaluate the thermal effects under suitable boundary conditions. CNL and CV conditions can be reasonably considered fundamental soil behaviour and used in the calibration of constitutive models, whereas the CNS condition represents a soil element in a certain problem-dependent condition.

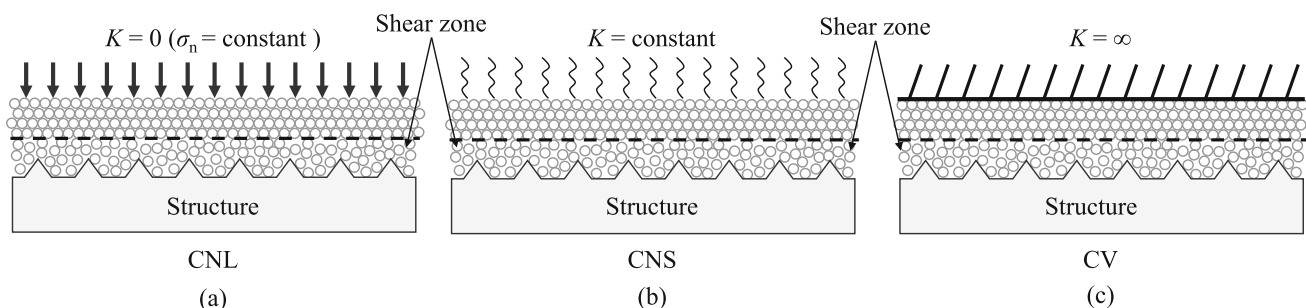


**Fig. 1** Schematic of boundary conditions normal to the soil interface: **a** constant normal load; **b** constant normal stiffness; **c** constant volume

At present, there has only been a limited amount of work investigating the impact of temperature on soil interfaces and the results exhibit some inconsistencies/variabilities, especially for clay–concrete interfaces. Direct shear tests on quartz sand [41, 42] and Fontainebleau sand [43, 44] subjected to CNL boundary conditions have suggested that sand–concrete interface behaviour is not affected in the temperature range of 5–60 °C. However, temperature effects on clay–concrete interfaces are less consistent. The friction angle (at the interface level) was found to be unchanged [44–47] or to decrease [41] with temperature. A more evident thermal influence was the increase in adhesion after heating, as observed with interfaces of illite [41], kaolin [44] and red clay [42], while the overconsolidated (OC) kaolin [45] and red clay [46] interfaces exhibited temperature independent adhesion. Yazdani et al. [48] observed that the shear strength of a kaolin interface subjected to heating was unchanged under a normal stress of 150 kPa, whereas the shear strength increased under normal stresses of 225 and 300 kPa. They concluded that the thermal strengthening was related to normal stress level, and not due to temperature effects.

Temperature has also been shown to affect the volumetric response of clay–concrete interfaces during shearing. It was observed from monotonic CNL and cyclic CNS shearing tests [41, 44] that the contraction of normally consolidated clay–concrete interfaces during shearing was reduced due to thermal consolidation, while this was not obvious in other experiments [46, 47].

Previous studies have mostly focussed on the monotonic temperature influence, especially heating, on the monotonic shearing behaviour of the soil interface, although the results show somewhat inconsistent trends. Moreover, limited data are available relating to thermal influences on cyclic shearing and undrained shearing behaviour of the soil–structure interface. Regarding these aspects, a comprehensive series of tests were performed using a well-calibrated temperature-controlled direct shear system, to investigate the shear response of interfaces within the temperature range of 2–38 °C (compatible with minimum and maximum temperatures that an energy pile may experience) under CNL, CNS and CV conditions. The void ratios of all samples were recorded, and the thermal influences on the volume change during shearing carefully examined considering the creep effect. The objective is to provide a comprehensive data set, which covers a large range of conditions to which energy geo-structures are subjected, and to draw conclusions on the overall shear behaviour of interfaces under various thermal and mechanical stress paths relevant for energy geo-structures.

## 2 Experimental setup and calibration

A modified direct shear apparatus manufactured by Wille Geotechnik was used in this study (Fig. 2a). The shear box was 10 cm × 10 cm × 3.2 cm and installed inside a thermally insulated carriage. As shearing proceeds, the extent of the shearing surface reduces continuously, and therefore, the effective surface area is used for calculating stresses. The load cap has a porous contact with the sample allowing water outflow (Fig. 2b). The lower part of the shear box was 1 cm in depth, with a porous stone at the bottom. A concrete block was embedded inside for the soil–concrete tests. The shearing platform was levelled via a bubble level, and the levelness was monitored throughout the tests. Vertical and horizontal displacements were measured by two linear variable differential transformers (LVDTs), with an accuracy of 0.001 mm. In this work, positive normal displacements signify contraction and negative signify dilation.

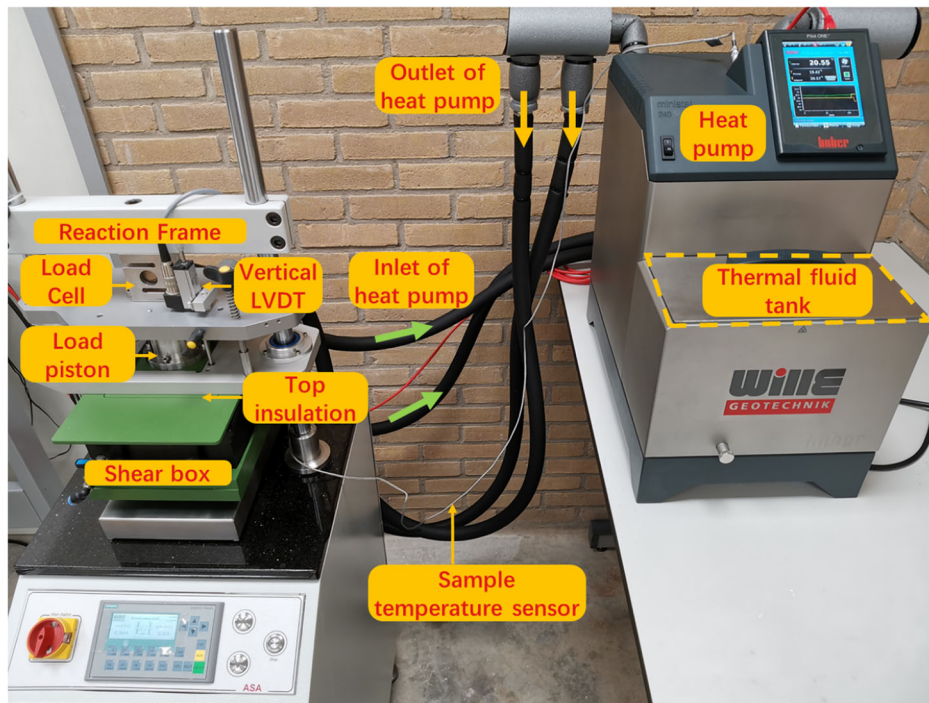
The thermal load was provided by a heat pump connected with two pairs of heat exchangers embedded in the load cap and the base of carriage (Fig. 2b). The temperature at the interface level was monitored by a PT100 sensor (TP 1, accuracy 0.1 °C) in the shear box, which was also used to control the heat pump. The load cap and the carriage were thermally insulated. Similarly, insulation lids were installed surrounding the shear box to prevent thermal loss and water evaporation, and thus, the temperature of the soil–concrete system was relatively uniform. The maximum temperature difference between the top insulation board and TP 1 was found less than 0.5 °C after thermal equilibrium. The whole system was kept in a climate room maintaining a constant temperature of  $20 \pm 2$  °C.

Considering that the magnitude of thermal influences on the volume change and the shear strength of a sample could be relatively small, the LVDTs and shear force measurements were carefully calibrated by imposing thermo-mechanical paths analogous to that in the subsequent experiments, using a dummy iron sample or the empty shear box. Details of the calibration process are presented in Appendix 2.

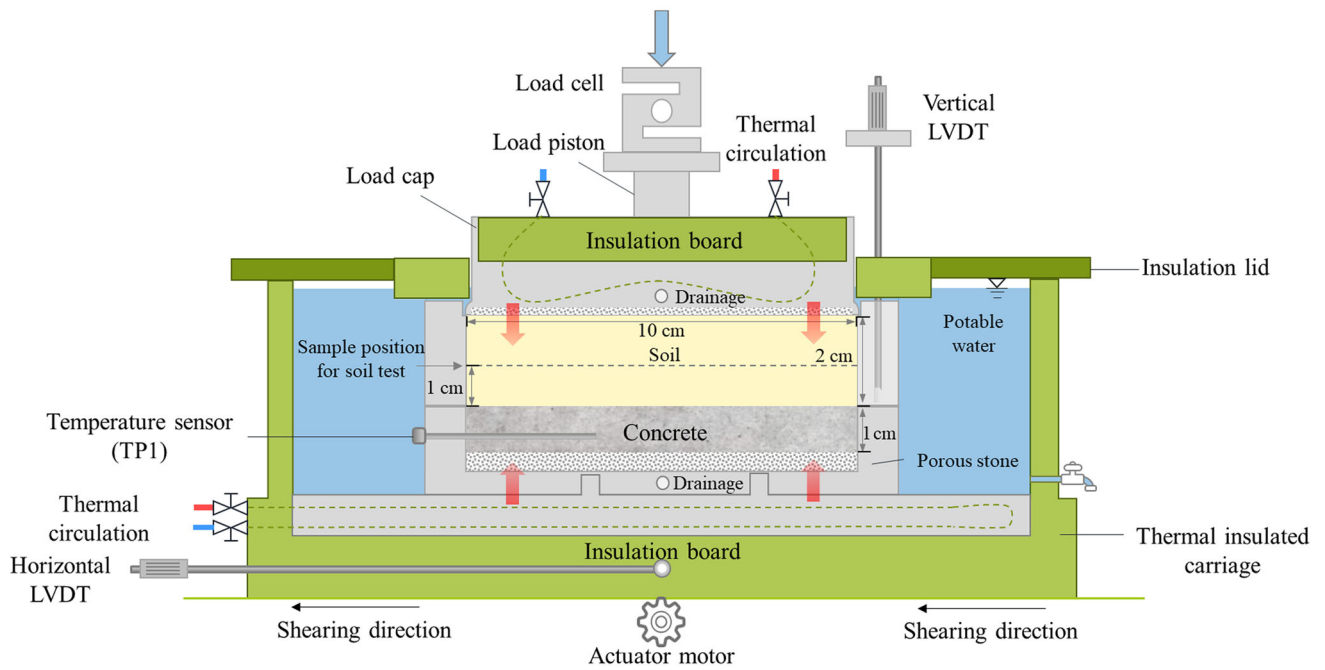
## 3 Material properties and sample preparation method

### 3.1 Sand

Geba sand, a commercial fine uniform silica sand, was used in this study. Its physical properties are given in Table 1. The size of particles ranged from 0.05 to 0.46 mm, and the grain-size distribution [49] is shown in Fig. 3. To prepare



(a)



(b)

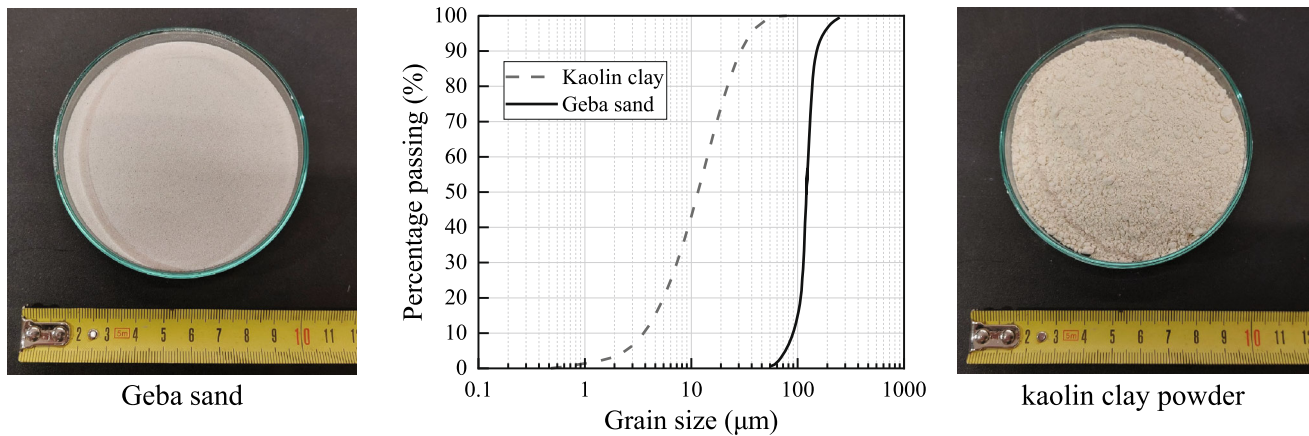
**Fig. 2** a Layout of temperature direct shear system; b schematic view of temperature-controlled direct shear box

the sample, the thermocouple (Fig. 2b) was first placed inside the shear box. Then, dry sand was poured uniformly and levelled with a 10 cm × 10 cm square tamper. A 20-mm-thick medium dense ( $D_r = 50\%$ ) sand sample, with

a targeted dry density of  $1.45 \text{ g/cm}^3$ , was reached by compaction.

**Table 1** Summary of physical properties of Geba sand [49] and kaolin clay

Geba sand	$C_u = D_{60}/D_{10}$	Minimum void ratio	Maximum void ratio	$D_{50}$ (mm)	Specific gravity ( $G_s$ )
	1.38	0.64	1.07	0.11	2.68
kaolin clay	LL(%)	PL(%)	$I_p$ (%)	Hydraulic conductivity (m/s)	Specific gravity ( $G_s$ )
	49.3	27.4	21.9	$10^{-8} \sim 10^{-9}$	2.65

**Fig. 3** Grain-size distribution of Geba sand and kaolin clay

### 3.2 Clay

Speswhite clay was used to investigate the thermo-mechanical behaviour of fine-grained soils. This clay consists of kaolinite with a small fraction of illite [50]. The Atterberg limits (Table 1) were measured in accordance with BS1377-2 [51], and its particle-size distribution (Fig. 3) was obtained via the laser diffraction method.

The samples were prepared by mixing kaolin powder with sufficient water to form a homogenous slurry with a water content of 1.5 liquid limit (LL). Then, the slurry was consolidated under 47.5 kPa in a large oedometer cell (diameter of 19 cm). After consolidation, samples of 10 cm × 10 cm × 2 cm were trimmed from the clay cake via a cutting ring. The water contents of samples varied between 47.6% and 48.5%. After lowering the sample into the shear box, the thermocouple was inserted into the sample.

### 3.3 Soil–concrete interface

For the interface tests, a 10 cm × 10 cm × 1 cm concrete block was first positioned in the lower shear box (Fig. 2b) followed by a similar procedure for preparing the soil

samples. The thermocouple was inserted through a pre-drilled hole inside the concrete block to record and control the temperature at the interface.

The surface of the concrete block was profiled via an optical stereo microscope along 5 lines in the shearing direction as illustrated in Fig. 4a. For each line, the average  $R_n$  over two measurements of 13 mm was calculated (Fig. 4b). Paikowsky et al. [20] suggested that values of  $R_n$  between 0.02 and 0.5 are categorised as “intermediate” roughness, which implies that a portion of the shear strength of the soil mobilises at the interface level.

## 4 Experimental programme

### 4.1 Test parameters for soil and soil interface

After preparation, samples were consolidated in the shear box at room temperature (20 °C). Initially, a normal contact force of 5 kPa was applied on the samples, and then, samples were submerged by distilled water [52] and left for 1–2 h. Then, the target normal stress was reached following the loading sequence of 25, 50, 100 and 150 kPa (stopping where required) prior to temperature variation. Each intermediate load step was maintained for 2 h. It

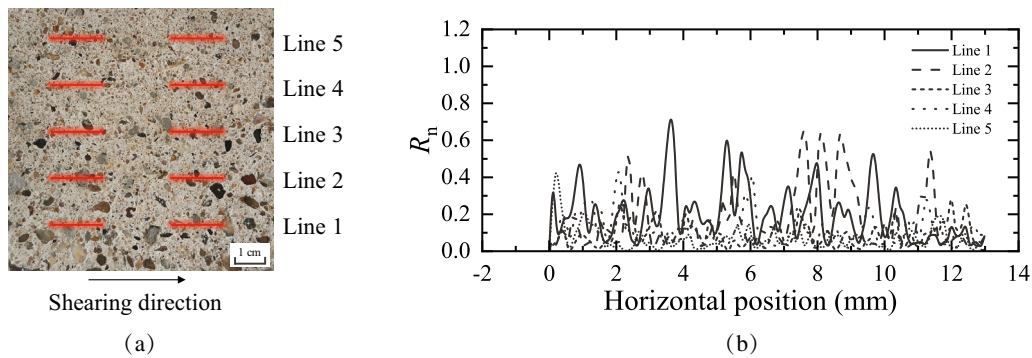


**Fig. 4** **a** Surface of the concrete block; **b** normalised roughness at different lines

should be noted that creep would proceed simultaneously during the temperature variation. Thus, the last consolidation step for isothermal tests was prolonged for the same duration used to achieve the target temperature in the parallel experiments. Any thermal or shearing load was imposed on the sample under a normally consolidated (NC) state.

The thermo-mechanical behaviour was investigated at ambient temperature (20 °C), 2 and 38 °C. Sand and sand interface samples were subjected to temperature variation and shearing at rates of 9 °C/h and 0.25 mm/min, respectively. For clay and clay interface tests, 3 °C/h for the monotonic thermal loading was chosen and 5 °C/h for thermal cycles to reduce the test duration. Insignificant excess pore pressure would be induced by such rates [41, 44, 45]. Based on the one-dimensional consolidation tests results of the clay samples subjected to normal stresses between 50–150 kPa, a shear rate of 0.26 mm/min was recommended [52]. Here, monotonic shear tests were conducted at 0.012 mm/min to ensure no excess pore pressure was generated. A shearing rate of 0.12 mm/min was selected for cyclic shearing after a comparison between the results of the two rates showing negligible differences.

## 4.2 Thermo-mechanical loading paths

The performed tests are categorised in four series:

*Series I: Temperature effect on the mechanical behaviour of soils and soil–concrete interface (Consolidation–Monotonic thermal loading–Monotonic shear (CNL)).*

The loading paths of these tests are depicted in Fig. 5a. Samples were first consolidated (path 0–1, where normal stresses,  $\sigma_n = 50, 100,$  and 150 kPa were selected), heated/cooled to 38 or 2 °C from the ambient temperature (20 °C) (path 1–1'/1''), followed by monotonic shearing with the normal stress kept constant (CNL).

*Series II: Effect of thermal cycles on the mechanical behaviour of soil–concrete interface (Consolidation–Cyclic thermal loading–Monotonic shear (CNL on sand–concrete interface/CV on clay–concrete interface)).*

Samples were first consolidated to normal stresses of 50 or 150 kPa (path 0–1). Then, samples were subjected to 5 heating or cooling cycles (path 1–1'/1'') varying, respectively, between 20 to 38 °C or 20 to 2 °C. After the thermal cycles, the sand–concrete samples were monotonically sheared under drained conditions at 20 °C, while the normal stress was kept constant (CNL). On the other hand, clay–concrete samples were sheared, while the total volume of the sample was kept constant (CV), to investigate the thermal cycle effect under undrained shearing conditions [37, 53]. The possible loading paths are shown in Fig. 5b.

*Series III: Temperature effect on the cyclic shear response of soil–concrete interface (Consolidation–Temperature change–Two-way cyclic shear (CNL)).*

The soil interface of an energy pile may experience cyclic mechanical shearing, due to the thermal elongation/shortening of the pile caused by the thermal loading. The distribution of shear displacement is highly dependent on the constraints from surrounding soils and the superstructure. Therefore, it is possible to identify a location along the length of the pile (also known as the null point) at which the magnitude of soil–structure displacement would be zero. Then, the magnitude of the soil–structure displacement increases from the null point towards the two ends of the pile in the opposite direction. Considering an extreme case, for example a floating pile, the null point is situated near the pile head and the pile tip would experience the largest displacement [54].

To identify a realistic magnitude of the shearing displacement, the temperature variation collected from a continuous operation GSHP system in Jiangsu Province, China, is presented in Fig. 6a. It can be inferred that energy piles may experience a temperature variation ( $\Delta T$ ) as large

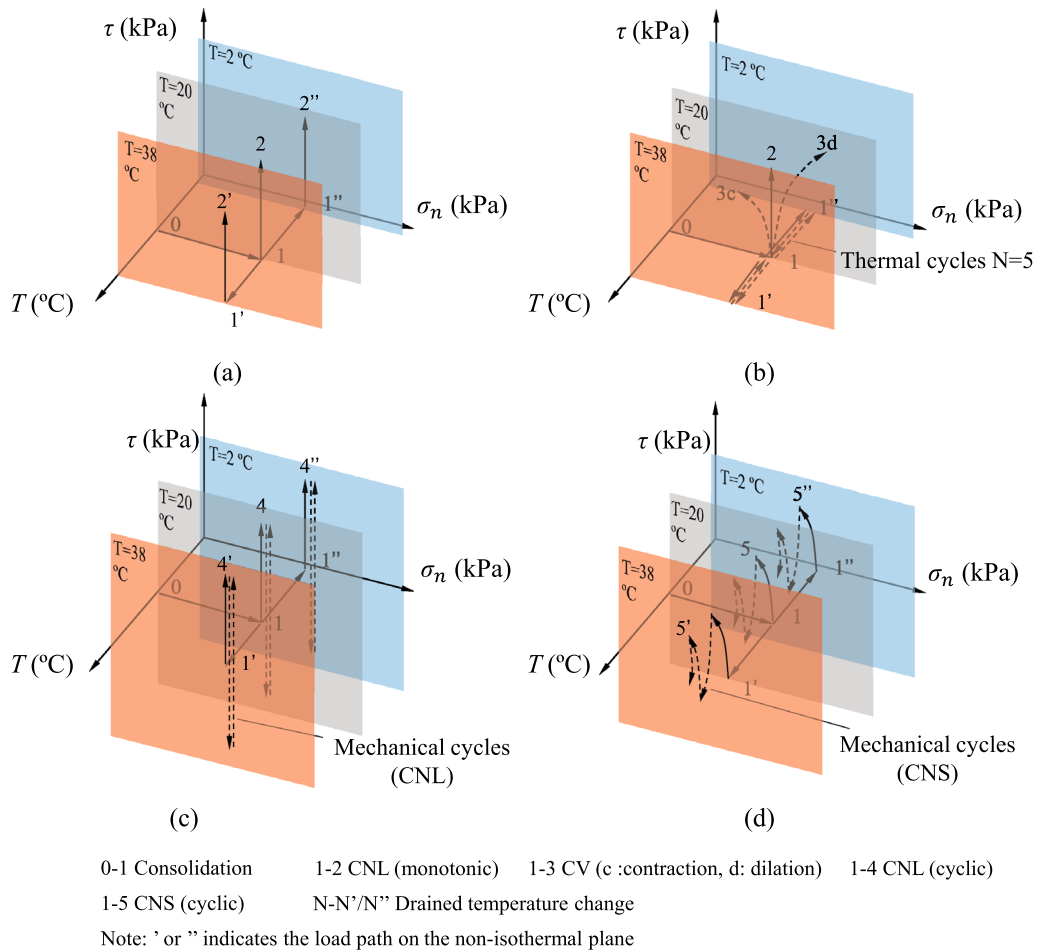


Fig. 5 Schematic diagram of thermo-mechanical load paths: **a** Series I; **b** Series II; **c** Series III; **d** Series IV

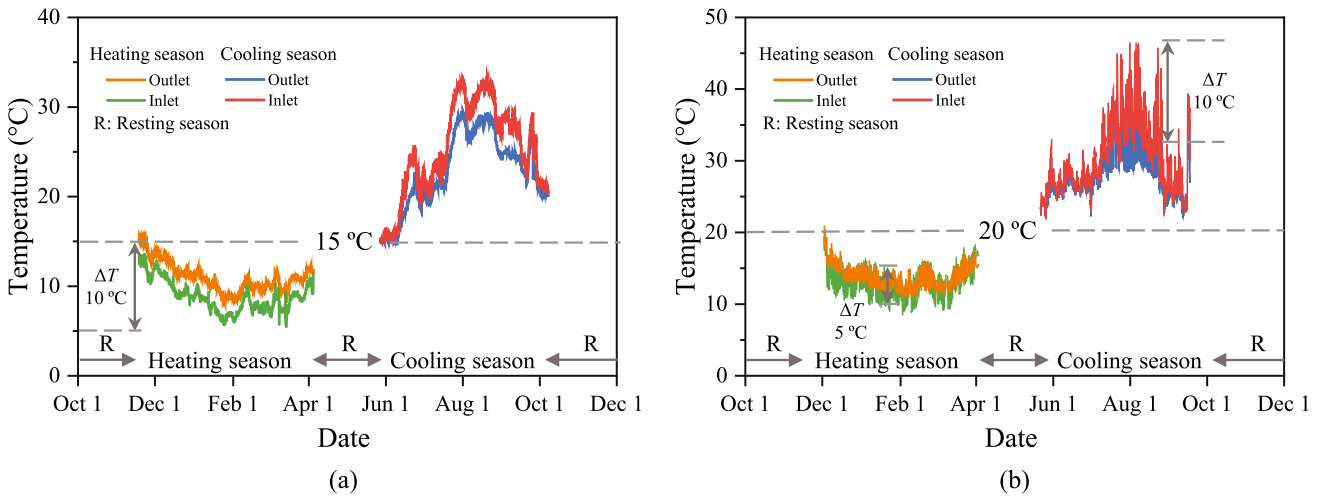


Fig. 6 Field monitoring data of inlet and outlet temperature of GSHP systems in Jiangsu Province, China. **a** Continuous operation system; **b** intermittent operation system

as 18 °C. Given a 20-m-long floating energy pile, the tip of the pile may experience a displacement of 4 mm in the upward and downward directions within a year. Such an

amount of displacement is also possible along longer piles with a lower degree of constraint at the head compared to its tip (e.g. a semi-floating pile).



To investigate the thermal effects under such a loading condition, samples were first consolidated to 150 kPa, then heated/cooled to 38 °C or 2 °C from 20 °C, followed by a series of two-way cyclic shearing tests with a displacement amplitude of  $\pm 4$  mm. CNL conditions were selected to represent (i) the fundamental soil shear strength in relation to different stress levels (which is most useful to describe the behaviour numerically) and (ii) long duration shear processes (e.g. a half year) for which due to creep processes the normal force on the pile could be reasonably constant. The loading paths of these tests are demonstrated in Fig. 5c.

*Series IV: Temperature effect on cyclic shear response of soil–concrete interface with CNS boundary conditions (Consolidation–Temperature change–One-way cyclic shear (CNS)).*

For an intermittent operation GSHP system, the daily thermal load is applied to the pile at a much higher rate. The temperature of the pile could change from the ground temperature to a maximum value of approximately 10 °C higher in a few hours as observed from another field monitoring record (Fig. 6b). In this case, a more rapid cyclic shearing would likely be imposed along the soil interface. Considering such loading condition, samples were consolidated to 150 kPa, and then, one-way cyclic interface shear tests with a maximum displacement of 2 mm were conducted at temperatures 2, 20 and 38 °C. Due to the relatively short duration of the shearing process (note, this is still much slower than for cyclic loading typically observed in offshore foundations), the surrounding soil is assumed to react elastically (and drained) to the volume changes at the interface, and thus, a CNS condition was chosen for this test series. Based on the elastic expanding cylinder theory [32], a range of  $K$  would be reasonable, e.g. 100–1200 kPa/mm [41], and therefore, a medium-level stiffness of  $K = 500$  kPa/mm was selected for the current qualitative investigation. Where creep is low, longer-duration thermal cycles can also be well represented by these conditions. The loading paths are presented in Fig. 5d.

## 5 Experimental results

To ensure the reliability of the test results, repeatability tests were conducted at 20 °C on Geba sand and kaolin clay specimens consolidated to 50 kPa, and the results are shown in Fig. 7. Although the parallel tests results were not perfectly overlapping, the maximum difference was 1.5 kPa for Geba sand and 1.8 kPa for kaolin clay which

are considered acceptable. This could be regarded as a reference for an overall accuracy of the experiment and only the variation beyond this accuracy could be considered as the consequence of thermal influences.

### 5.1 Series IA: Temperature effect on the soils

The test results for sand–sand and clay–clay shearing are presented in Fig. 8. The shear stress vs. shear displacement responses (Fig. 8a, d) demonstrates that temperature has a negligible effect on the drained shearing behaviour in terms of ultimate shear strength. The ultimate shear stresses and the corresponding normal stresses were linearly correlated and are shown in Fig. 8b, e. The average peak friction angles obtained from the best-fitted line for the sand and clay were 33.90° and 20.87°, respectively. The average apparent cohesion for clay was 4.79 kPa. The difference between the friction angles at three levels of temperature was less than 1° for the two soils, which suggests a negligible influence of the temperature variation on the shear behaviour.

Normal displacement vs. shear displacement curves of soil–soil interface shearing are presented in Fig. 8c, f. The thermal effects on the normal displacements vs. shear displacements for sand and clay at different temperatures are not obvious. The reason is hypothesised to be that the thermally induced volume change is relatively insignificant compared to the pre-shear void ratio differences (due to sample preparation). The volume changes of each sample during temperature variation differed depending on the material (sand or clay), normal stress level, creep, and thermal load direction (i.e. heating or cooling), with hypotheses for the underlying cause discussed in more detail in Sect. 5.3. For brevity, the evolutions of volume change in the heating/cooling process for each sample were not presented, as they were almost identical as the first half cycle from the cyclic results presented in Figs. 10 and 13. Overall, for sand specimens, the maximum thermally induced volume strain was less than 0.1%, equal to a void ratio change ( $\Delta e$ ) around 0.002. For clay specimens, the maximum volume strain developed during heating, and was about 0.08% corresponding to  $\Delta e \approx 0.001$  (comparable to experiments in the literature [4, 9, 55]). These volume changes are less than the variation of initial void ratio ( $e_0$ ) after sample preparation (see Table 2, Appendix 1). The specimens with a higher void ratio contracted slightly more during shearing, and therefore, the differences of initial state (even when small) become significant and make the thermal influence, if any, harder to identify.

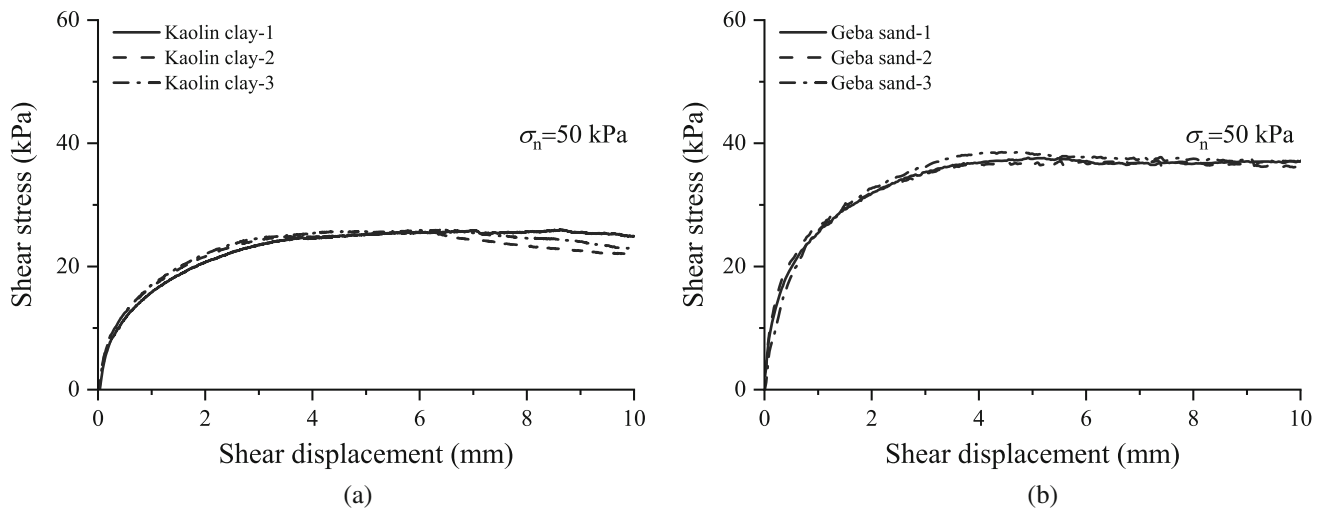


Fig. 7 Repeatability tests: **a** Geba sand and **b** kaolin clay

## 5.2 Series IB: Temperature effect on the soil–concrete interfaces

The corresponding tests results for a soil–concrete interface are presented in Fig. 9. The sand–concrete interface exhibited a hardening behaviour and mobilised  $80 \pm 3\%$  of the ultimate shear strength of the sand tests. The volumetric response (Fig. 9c) of the sand–concrete interface is dominantly contractive, compared to the sand–sand shearing behaviour (Fig. 8c), indicating that more sliding of the soil grains occurred along the interface [56]. For the results at  $2^\circ\text{C}$ , the mobilised shear stresses matched very well with that at  $20^\circ\text{C}$  and represent a friction angle of  $26.3^\circ$ . For shearing tests at  $38^\circ\text{C}$ , although a slight increase on the mobilised shear stress was observed (Fig. 9a, b), similar to the observations from Vasilescu et al. [57], the differences were within the accuracy of the direct shear apparatus and were too small to be considered as the consequence of temperature. It can be concluded that the effect of temperature on the sand–concrete interfaces, in the studied range, can be neglected for practical purposes.

In Fig. 9d–f, the test results related to clay–concrete interface shearing are presented. A strain hardening mechanism was observed at the clay–concrete interface until a peak shear stress was mobilised at shear displacements of 1.5–2.5 mm, after which a strain softening mechanism was followed. This behaviour indicates that failure occurs at the interface level and can be attributed to the sliding of clay particles along the interface [58]. The average peak and ultimate shear stresses were about 82% and 68% of those mobilised at the clay–clay interface, respectively. Figure 9d and e shows a negligible effect of temperature on the peak shear stresses and the ultimate shear stresses.

The limited clay–concrete interface studies [44, 45, 48, 59] also indicate a small variation of the friction angle with temperature, in agreement with this study. However, the temperature effects on adhesion differ between studies. The change of the liquid film thickness could explain such a difference [46]. The viscous impulse ( $I_v$ ) for two circular interfaces bridged by a fluid film may be given by [60]:

$$I_v = \frac{16\eta R^3}{3ht_s} \quad (3)$$

where  $\eta$  is the dynamic viscosity of the thin liquid film along the interface,  $h$  is the thickness of the liquid film,  $t_s$  is the shearing time, and  $R$  is the circular meniscus radius. This indicates that adhesion is related to the change of  $\eta$  and  $h$ . The temperature variations in previous studies were similar ( $\Delta T = 20\text{--}30^\circ\text{C}$ ) yielding a comparable change of water viscosity. The different adhesions could have resulted from  $\Delta h$ , which strongly depends on how clay fabric rearranges during temperature variation. The thermal response of the clay fabric is known to be stress history dependent. For NC clay [41, 46], the collapse of clay fabric during thermal consolidation would reduce the  $h$  and increase the adhesion. For an OC soil during heating [45] or a NC soil during a cooling process [44], the arrangement of clay fabric is considered to be dispersed or unchanged, and thus, the cohesion is found to slightly drop or to be unchanged after heating. Meanwhile, the physicochemical mechanisms proposed by [61] suggested that soils with higher plasticity would undergo greater volume change during heating because of their higher chemical reactivity. Due to the low-medium plasticity clay used in this study, it experienced a relatively low volume change during temperature change (details addressed in the next section) and

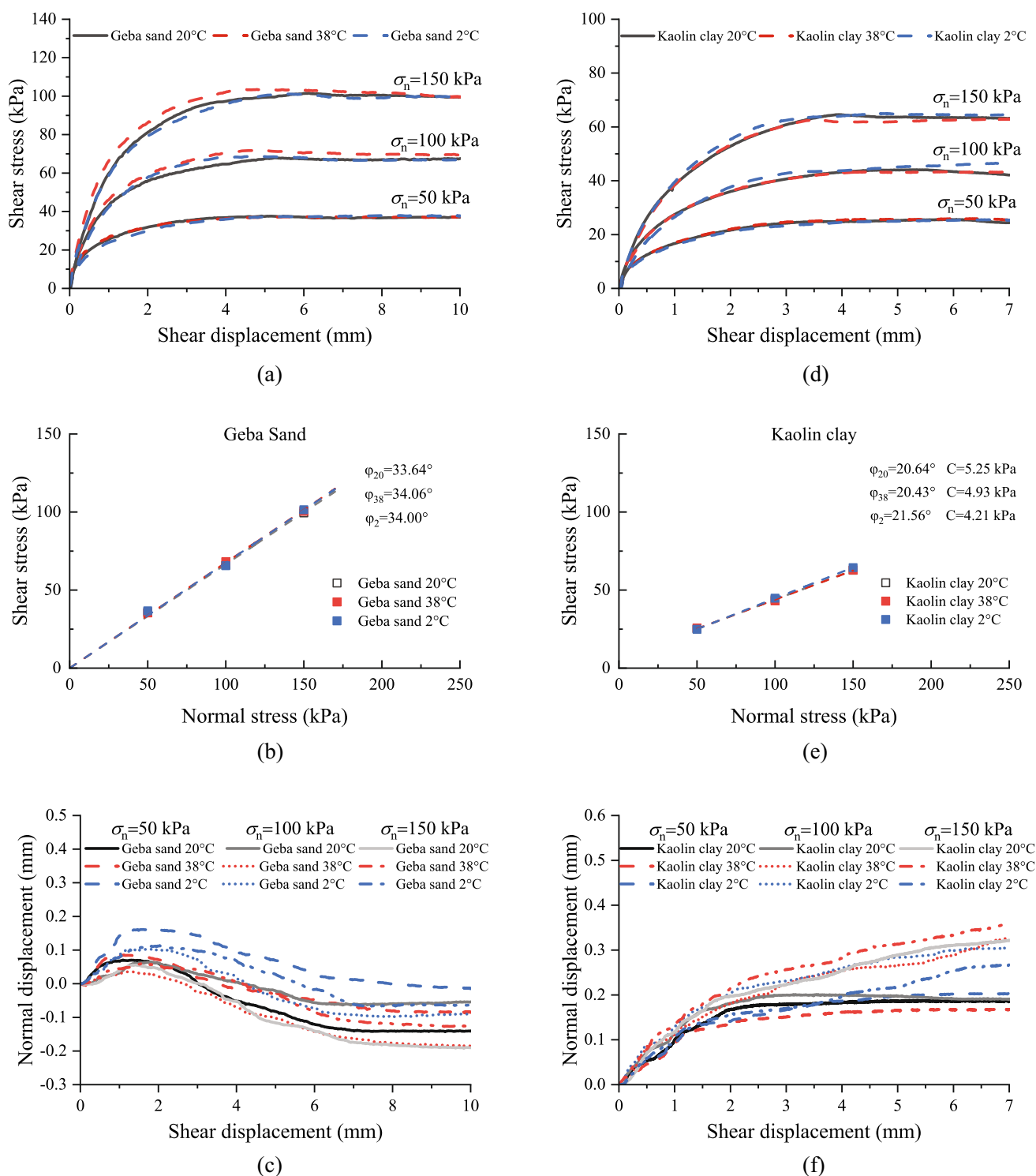


**Fig. 8** CNL results for soil samples at  $T = 2, 20, 38$  °C. Geba sand: **a** shear stress vs. shear displacement; **b** failure envelopes; **c** normal displacement vs. shear displacement; kaolin clay: **d** shear stress vs. shear displacement; **e** failure envelopes; **f** normal displacement vs. shear displacement

thus exhibited a small variation of adhesion due to temperature change.

The temperature effects on the normal displacement response during shearing are again almost indistinguishable

(Fig. 9c and f), which is suggested to be for the same reason as for the soil tests.

### 5.3 Series II: Effect of thermal cycles on the soil–concrete interface

Figure 10 shows the volume change and temperature variation (recorded by TP 1) in sand–concrete interfaces during heating/cooling cycles at normal stresses of 50 and 150 kPa. Thermo-elastic behaviour was assumed for the concrete block ( $\alpha = 1.2 \times 10^{-5}/^\circ\text{C}$ ), and its thermal vertical deformation was removed during data processing. Due to a relatively low rate of temperature change, it was essential to consider creep effects [62] in the interpretation of data to reveal the net influence of thermal cycles. The secondary compression index ( $C_{\alpha e}$ ) is defined as [63]:

$$C_{\alpha e} = -de/d(\log t) \quad (4)$$

where  $t$  is the elapsed time of the secondary compression. Accordingly, the volumetric strain during thermal cycles caused by creep (dashed line in Fig. 10) was estimated by extending the logarithmic fitting of the deformation after the completion of the primary consolidation assuming a temperature independent  $C_{\alpha e}$ . Examples of the consolidation process are provided in Appendix 3.

Under the lower normal stress (50 kPa), both heating and cooling cycle-induced plastic strains in addition to creep (Fig. 10a, b), mainly observed within the initial 1–2 thermal cycles. A thermo-elastic response is also seen via the strain fluctuating with temperature. Under the higher normal stress (150 kPa), the observed deformations (Fig. 10c, d) are virtually identical with the estimated creep throughout the test, with the thermo-elastic fluctuation still observed. The thermo-plastic strains at the end of each cycle are presented in Fig. 11a, after the subtraction of the estimated creep from the total deformation. It can be inferred that the thermally induced plastic strain was dependent on vertical stress and becomes less significant under higher normal stress (150 kPa).

This behaviour is different from the established theory for clay [64–66], which assumes thermo-plastic strain is dependent on the thermal loading direction. The observed phenomenon can be explained from a micro-mechanism that may occur in sand. The external load is mainly carried by the “*strong force network*” of particles with larger inter-particle forces, while the rest (up to 60% [67]) carries small load constituting the “*weak cluster*” [63]. Under lower normal stress, the contact between grains could be relatively lose with some unstable voids [68]. When temperature changes, the thermal-elastic deformation of grains could be sufficient to trigger the rearrangement of the soil skeleton, resulting in a macro-scale deformation. However, under higher confinement, sand particles forming strong chain-forces are more stable and less influenced by thermal agitation.

After the thermal cycles, the sand–concrete interface samples were sheared to 10 mm and compared with the isothermal tests. Figure 12a shows that the effects of heating/cooling cycles, prior to shearing, are negligible on the mobilised shear stress at the interface level. Some unexpected abrasion happened on the concrete surface during the sample preparation for the cooling cycle test and it led to a small strength increase. The test was thus repeated under 20 °C (dashed grey line) to verify such an increase was not caused by the thermal cycles.

The volumetric strains of the clay–concrete interface samples subjected to heating/cooling cycles are shown in Fig. 13. The creep effect was estimated in the same way as for the sand–concrete interface programme. During the cooling cycles, the volume change followed the trend of secondary consolidation and showed a nearly thermo-elastic response (Fig. 13b, d). For the heating cycle tests, irreversible contraction was mainly induced during the first 2–3 cycles, after which it kept increasing at a lower rate. The thermo-plastic deformation for each cycle is plotted in Fig. 11b. The thermo-elastic deformation became more visible in the 4–5th cycles (Fig. 13a, c) because of the lower plastic strains generated. As opposed to the thermal cycle effects observed in the sand–concrete interface samples, in clay–concrete interface samples, the higher vertical stress resulted in larger thermo-plastic strains. This volumetric response of the clay–concrete interface follows what has been observed in clays [64, 65].

After the heating/cooling cycles, the clay–concrete samples were sheared under CV conditions (resembling undrained conditions). The variation of shear stress against normal stress is shown in Fig. 14a. To ensure the only variable between the parallel CV shearing tests was the thermal history, two isothermal specimens were consolidated under 150 kPa for 35 h (equal to the duration of the thermal cycles) and 2 h, respectively. During shearing, the former behaved stiffer (the black line labelled with “20 °C, 35 h” in Fig. 14b), indicating that the creep process does influence the subsequent shearing and therefore was selected as the reference. Figure 14a shows that heating/cooling cycles have a significant effect on the clay–concrete interface and this effect is more pronounced at higher stresses. All samples experienced a normal stress reduction during shearing, where the maximum change was in the isothermal sample and the minimum change was in the sample after heating cycles. The reduction of normal stress in the CV conditions implies contraction and therefore the generation of positive pore water pressures. Therefore, the shear stress versus (effective) normal stress curves of the interface experiments resemble the stress path (deviatoric stress versus mean effective stress) of undrained triaxial experiments on clays samples [5, 10, 69–71]. The peak and residual failure envelopes obtained from

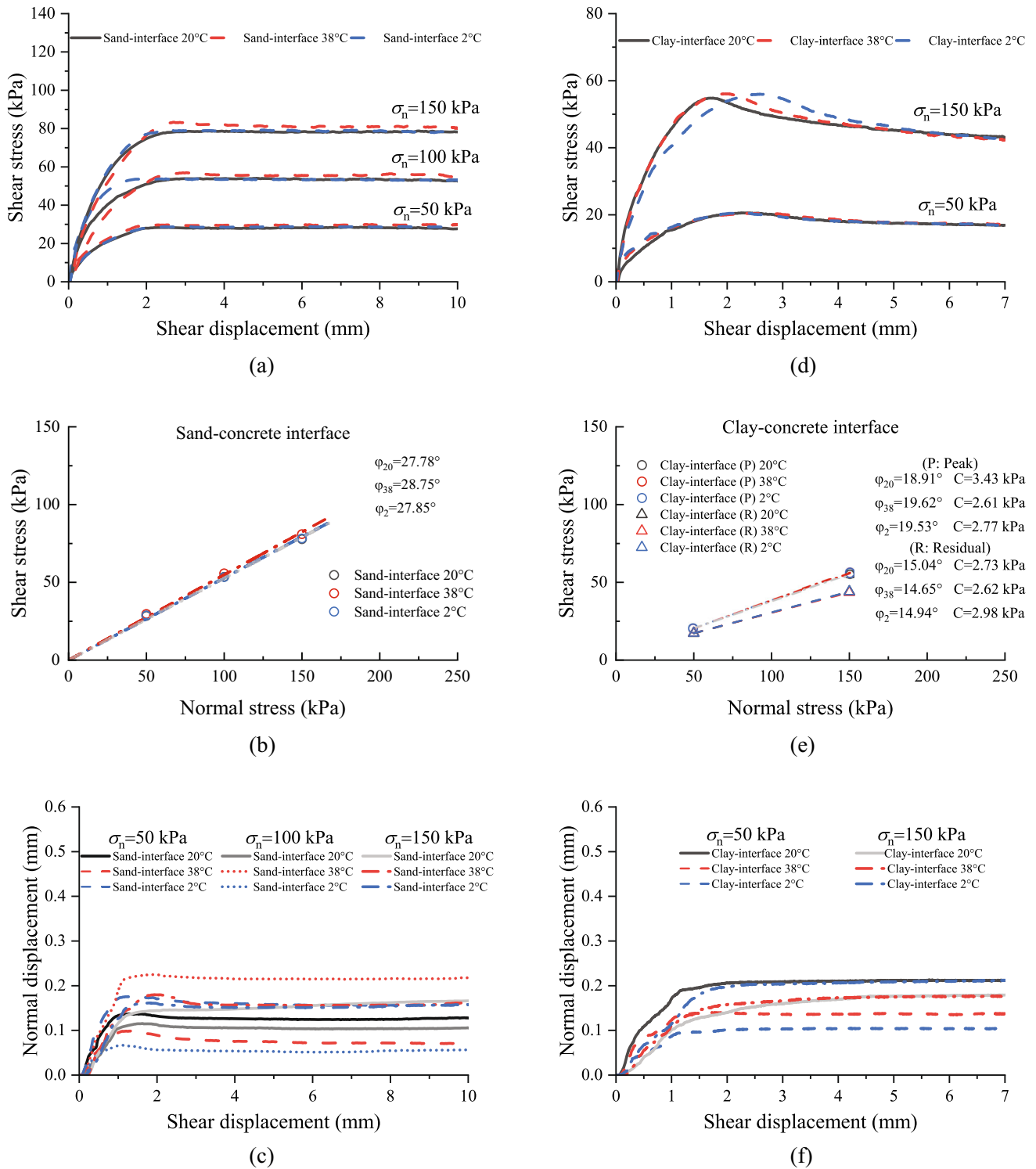


**Fig. 9** CNL results for soil interface samples at  $T = 2, 20, 38$  °C. Geba sand–concrete interface: **a** shear stress vs. shear displacement; **b** failure envelopes; **c** normal displacement vs. shear displacement; kaolin clay–concrete interface: **d** shear stress vs. shear displacement; **e** failure envelopes; **f** normal displacement vs. shear displacement

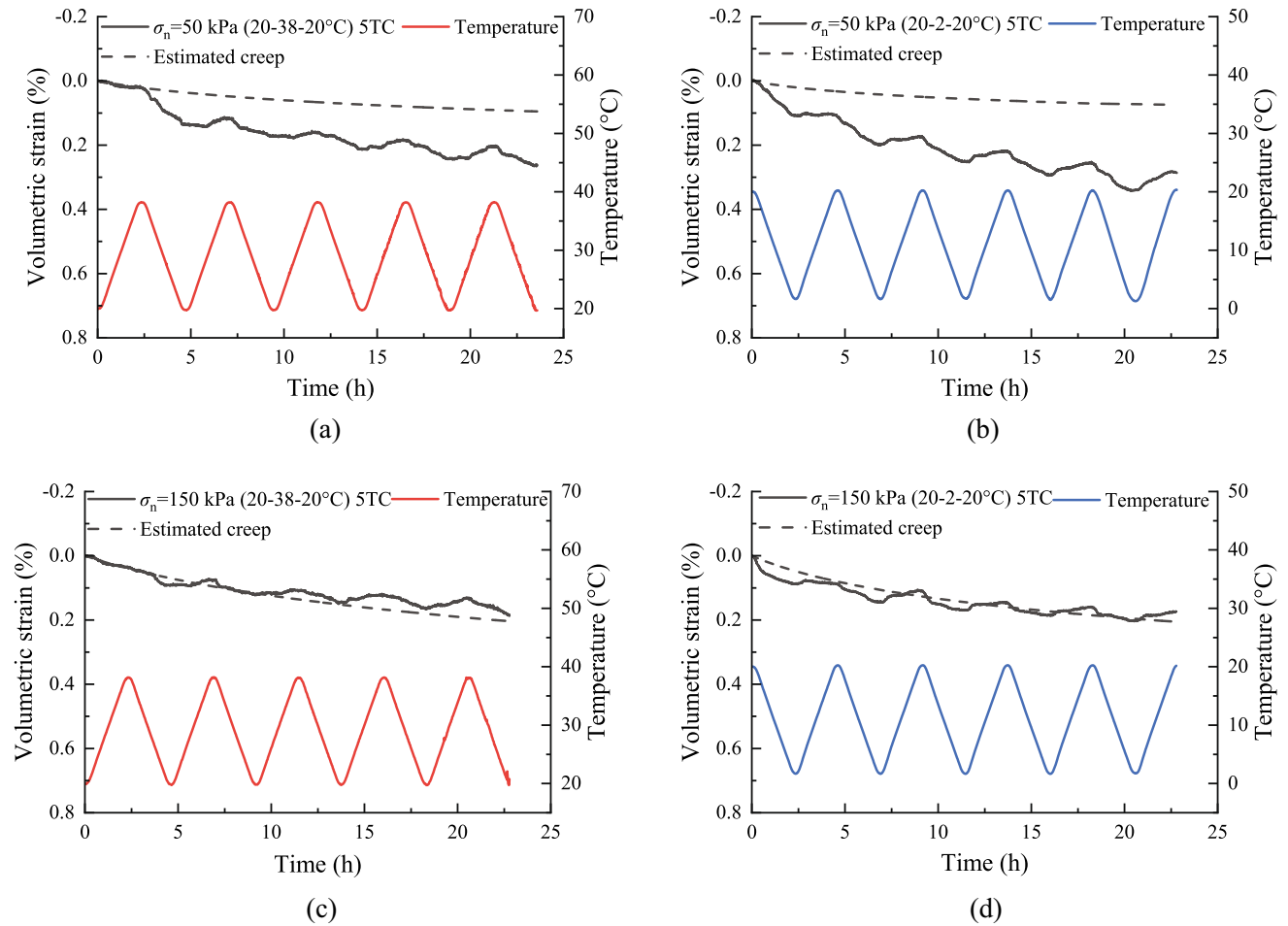


**Fig. 10** Volume change of sand–concrete interface during thermal cycles: **a** heating cycles at 50 kPa; **b** cooling cycles at 50 kPa; **c** heating cycles at 150 kPa; **d** cooling cycles at 150 kPa

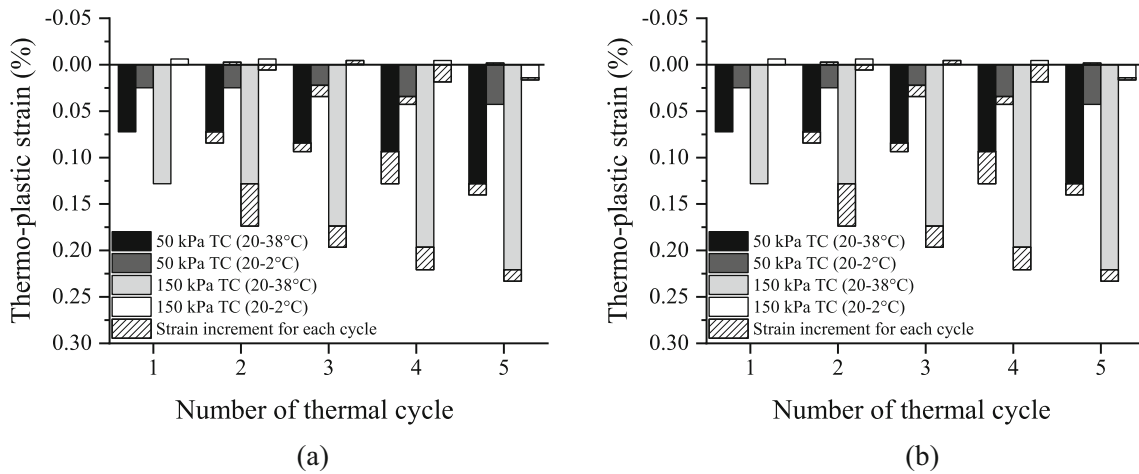


**Fig. 11** Accumulated thermo-plastic strain after the completion of each thermal cycle: **a** sand–concrete interface; **b** clay–concrete interface

isothermal tests (Fig. 9e) are considered to fit well with the CV shear results. Therefore, the strength parameters of the clay–concrete interface are considered to be independent of the temperature history.

For the sample consolidated at a normal stress of 150 kPa and subjected to heating cycles (shown by red solid line), the stress path started to evolve vertically (kept constant) at the beginning of shearing before bending

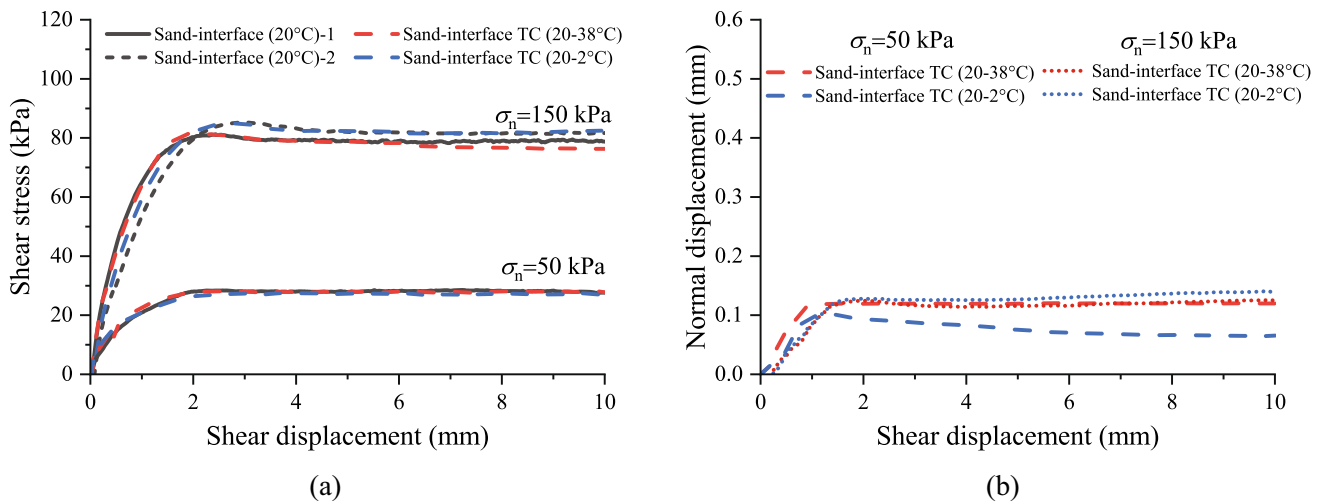


**Fig. 12** CNL results for sand–concrete interface after heating/cooling cycles: **a** shear stress vs. shear displacement; **b** normal displacement vs. shear displacement

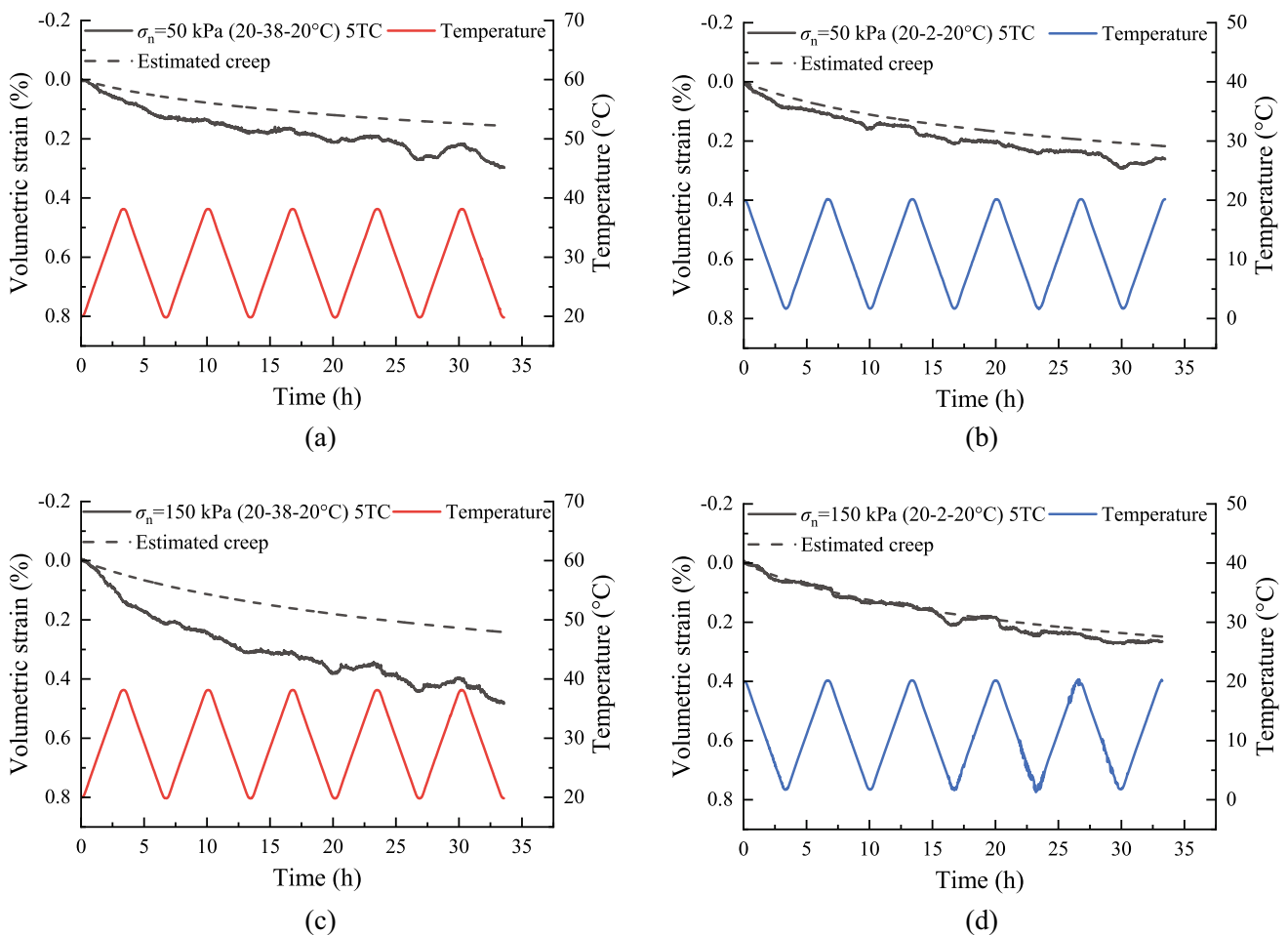


**Fig. 13** Volume change of clay–concrete interface during thermal cycles: **a** heating cycles at 50 kPa; **b** cooling cycles at 50 kPa; **c** heating cycles at 150 kPa; **d** cooling cycles at 150 kPa

towards the peak failure envelope. Based on critical state soil mechanics, such a stress path implies a typical OC soil

response, suggesting an expanded yield surface after heating cycles, and would imply lower pore pressure

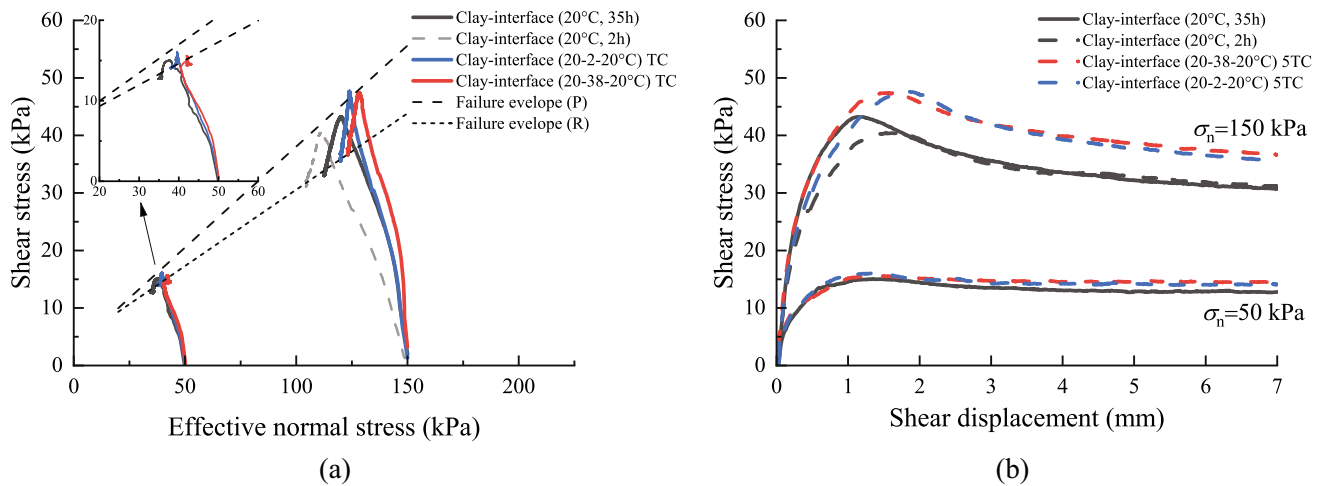


**Fig. 14** Constant volume shearing results for clay–concrete interface tests after thermal cycles: **a** shear stress vs. effective normal stress; **b** shear stress vs. shear displacement. The labels “20 °C, 35 h” and “20 °C, 2 h” indicate the consolidation duration for the isothermal samples

generation in field conditions. In contrast, the path after cooling cycles mostly overlapped with the isothermal one, and the vertical stress decreased immediately after the shearing started. Such a trajectory, without the ‘vertical’ segment, implies the stress state remains NC. It is assumed in many constitutive models [65, 72, 73] that the yield surface will expand during drained heating, and therefore be larger when the soil returns to the ambient temperature, while cooling cycles would not alter the size of the yield surface. Therefore, it appears that the thermo-mechanical response of a clay–concrete interface may also be characterised in the framework of critical state soil mechanics with a temperature-dependent yield locus.

#### 5.4 Series III: Temperature effect on the cyclic shear response of soil–concrete interface layer

The sand–concrete interfaces were subjected to 30 two-way shearing cycles at three temperatures (2, 20 and 38 °C). For clarity, only the results of cycle numbers 1, 5, 29 and 30 are presented in Fig. 15a, c. In the first cycle (at all temperatures in Fig. 15a, b), the maximum shear stress reached 88 kPa, which is similar to the value observed for the monotonic shearing tests. For the rest of the cycles, the shear stress decreased and then stabilised at 85 kPa. The shear responses at different temperatures were very similar indicating a negligible thermal effect of the shear strength and stiffness under cyclic CNL shearing.

The normal displacement against shear displacement forms a hysteresis loop (Fig. 15c) and the sample volume continued to reduce as the cyclic shearing proceeded (Fig. 15d). The net contraction at each shearing cycle decreased with increasing cycles, and almost 60% of the contraction was accumulated in the first 5 cycles.

Comparing the volume changes at different temperatures, the sand–concrete interface samples at 2 and 20 °C, respectively, experienced the highest and the least accumulated volume reduction (Fig. 15d). This may be for two reasons: temperature effects, and the pre-shear void ratios, which were 0.821, 0.847 and 0.831, respectively, for the interface elements sheared at 20, 38 and 2 °C. The sample sheared at 20 °C had the smallest pre-shear void ratio and thus exhibited less contraction due to shearing. The interface sample sheared at 2 °C, while having a lower pre-shear void ratio compared to the interface sample sheared at 38 °C, experienced a higher volume change during cyclic shearing. This behaviour may reflect the effect of temperature on the volumetric behaviour.

The same test programme was performed on clay–concrete interface samples for 10 cycles, and the results are shown in Fig. 16. For all three interface specimens, sheared at 2, 20 and 38 °C, the shear stresses peaked at 57 kPa and then decreased to 48 kPa at + 4 mm within the first cycle (Fig. 16a). As the shearing cycle continued, the peak shear stresses decreased to 46 kPa, with the residual shear stress stabilised at  $\pm 37$  kPa after the 3rd cycle (Fig. 16b). Although the peak shear stresses were reached at different shear displacements in the 1st cycle (Fig. 16a), the difference was eliminated in subsequent cycles (i.e., 2nd, 5th and 10th). Thus, the temperature influences on the cyclic peak shear and residual shear strengths are again observed to be insignificant.

The accumulated volume changes during the cycles are depicted in Fig. 16c, d. The volume change was significant at the beginning and then kept increasing with a lower rate as the shearing proceeded. Up to 60% of the total deformation was accumulated within the first 1.5 cycles (Fig. 16d). The specimen sheared at 20 °C experienced the largest net contraction within most of the cycles. This



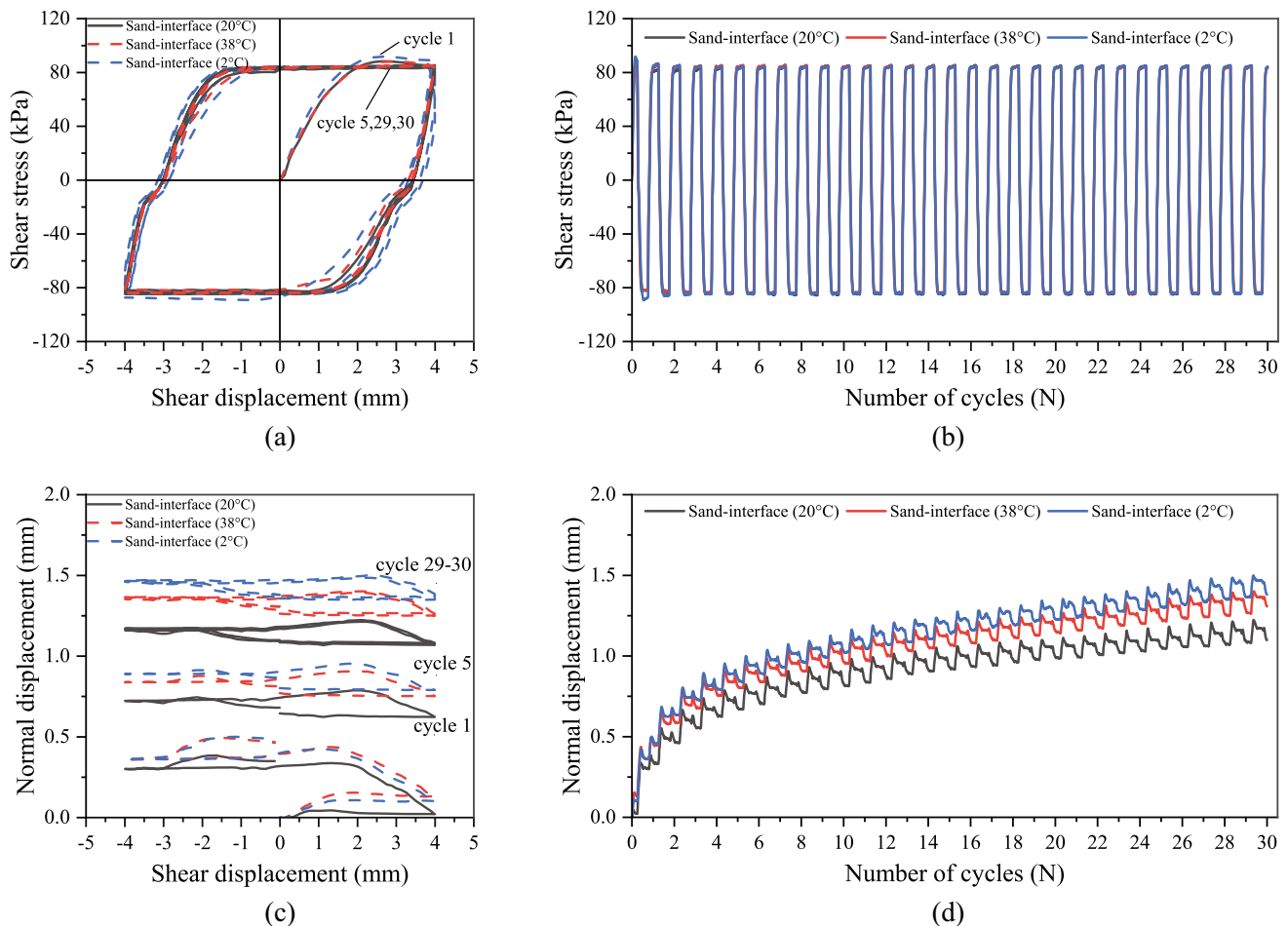


**Fig. 15** Two-way cyclic shearing tests of sand–concrete interface at  $T = 2, 20, 38\text{ }^{\circ}\text{C}$  under CNL (150 kPa) condition: **a** shear stress vs. displacement; **b** shear stress vs. cycle number; **c** normal displacement vs. shear displacement; **d** normal displacement vs. cycle number

result reflects that the temperature change could (partially) mitigate the contraction during cyclic shearing, while this was not observed in monotonic shearing (the first 1/4 cycle in Fig. 16c). Note that the pre-shear void ratio for clay–concrete interface samples sheared at 20, 38 and 2 °C was 0.959, 0.964 and 0.961, respectively, which would not explain this behaviour. This observation requires further confirmation before firm conclusions can be made.

### 5.5 Series IV: Temperature effect on cyclic shear response of soil–concrete interfaces with CNS boundary conditions

The test results of the sand–concrete interface for Series IV are summarised in Fig. 17. Due to the relative contractive characteristic of medium-dense sand during shearing, the normal stress and mobilised shear strengths reduced significantly within the first 1–2 cycles (Fig. 17a, b) where most of the normal displacement occurred (Fig. 17c). Similar stress paths were observed for tests at 2, 20 and 38 °C. These stress paths varied inside a failure envelope

(Fig. 17a) and with a slope determined to be 0.56, which is identical to the stress ratio ( $\tau/\sigma_n$ ) derived from the cyclic CNL tests. Thus, the temperature is seen to have negligible influence on the cyclic friction angle of the sand–concrete interface, regardless of the boundary conditions. The temperature effect on the volumetric response (Fig. 17d) was not distinguishable because sand-interfaces tend to approach the  $e_{\min}$  state of sand during cyclic CNS shearing [74]. Thus, in real thermo-active geo-structure applications, the possible strength degradation of the sand–structure interface can be evaluated without considering the direct thermal behaviour of the interface. It is noted that, for thermo-active pile foundations with the tip located in a sand, the majority of the bearing strength would be derived from tip resistance.

The shearing responses for the clay–concrete interface are shown in Fig. 18. The normal stresses and shear stresses decreased gradually under CNS shearing (Fig. 18a, b). The stress paths under three levels of temperature were bounded at the peak shear stress envelope rather than the residual strength envelope (Fig. 18a) derived from the

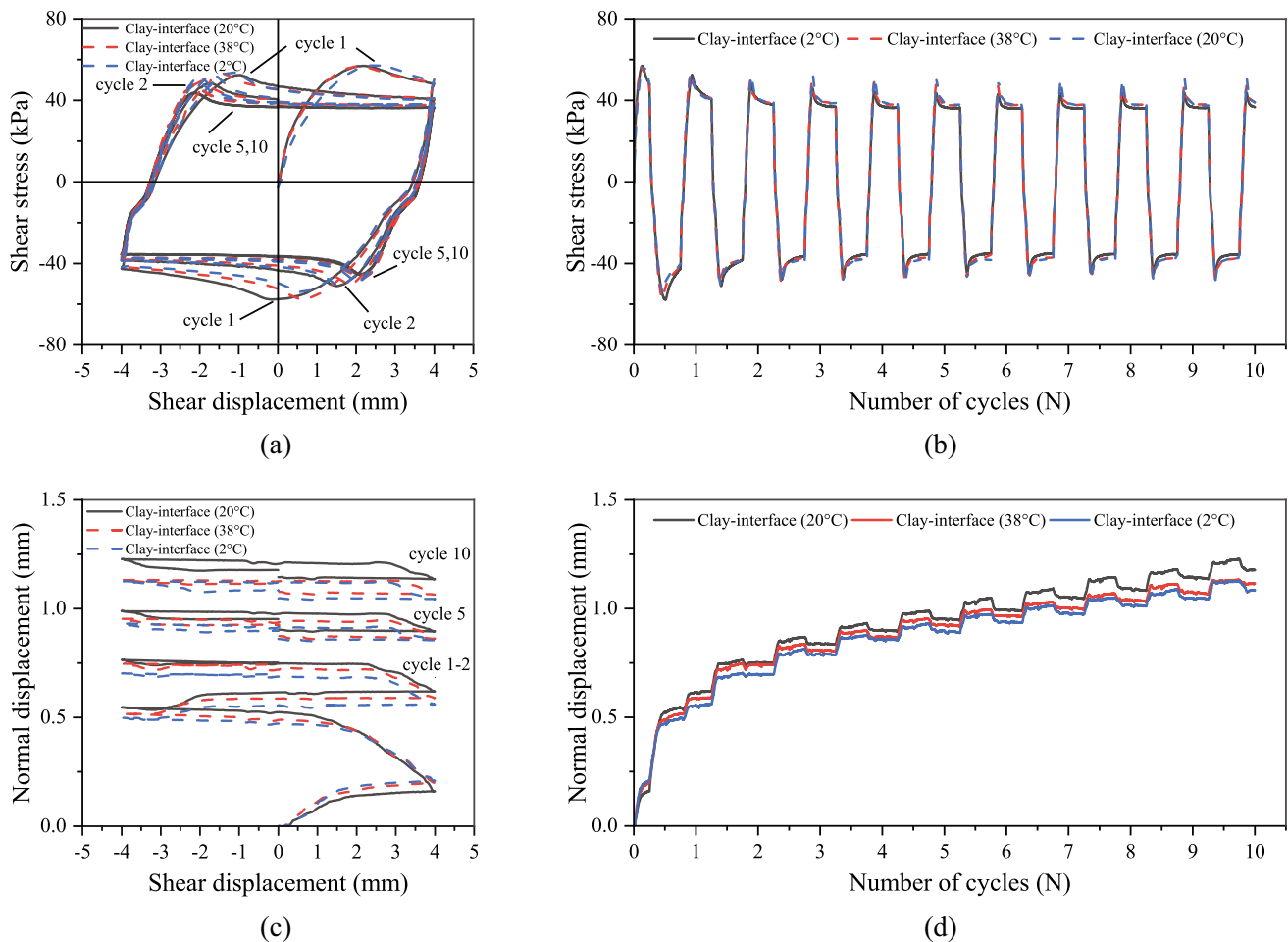


**Fig. 16** Two-way cyclic shearing tests of clay–concrete interface at  $T = 2, 20, 38\text{ }^{\circ}\text{C}$  under CNL (150 kPa) condition: **a** shear stress vs. displacement; **b** shear stress vs. cycle number; **c** normal displacement vs. shear displacement; **d** normal displacement vs. cycle number

monotonic tests (Fig. 9e), indicating temperature-independent strength parameters in cyclic CNS shearing. The rate of degradation (Fig. 18b) is far less than that of the sand-interface (Fig. 17b), as the normal stress and shear stress of the sample sheared at  $20\text{ }^{\circ}\text{C}$  remained at 56 kPa and 21 kPa, respectively, after 10 shearing cycles. Moreover, the degradation tended to stabilise in the last few cycles.

The stress paths of the samples sheared at 38 and  $2\text{ }^{\circ}\text{C}$  (Fig. 18a) converged with the stress path of the sample sheared at  $20\text{ }^{\circ}\text{C}$  in the first 1–2 cycles, but progressively shifted towards the right side with increasing cycles suggesting a lower reduction in the normal stress, consistent with the observations made in Sect. 5.4. As the frictional coefficient remained unchanged, the shear stress degradation is closely associated with the volumetric behaviour at different temperatures (Fig. 18c, d). The pre-sheared void ratio cannot be overlooked to draw a rigorous statement on the temperature effect. Note that the void ratios before shearing were 0.964, 0.963, 0.948 for specimens sheared at 20, 38 and  $2\text{ }^{\circ}\text{C}$ . The differences of the initial state between

20 and  $38\text{ }^{\circ}\text{C}$  specimens can be safely ignored, and thus, heating process can be again seen to partially mitigate the contraction during cyclic CNS shearing.

## 6 Conclusions

The shearing behaviour of soil interfaces was investigated via a series of temperature-controlled direct shear tests. These were conducted within a temperature range of  $2\text{--}38\text{ }^{\circ}\text{C}$  and a normal stress range of 50–150 kPa, thereby covering the most common operating conditions of GSHP applications. Based on this study, the following conclusions can be drawn:

- (1) The strength parameters of the sand and clay interface may reasonably be considered as constant within the relatively mild temperature range typical of energy structure applications under various boundary conditions (e.g., CNL, CNS and CV).

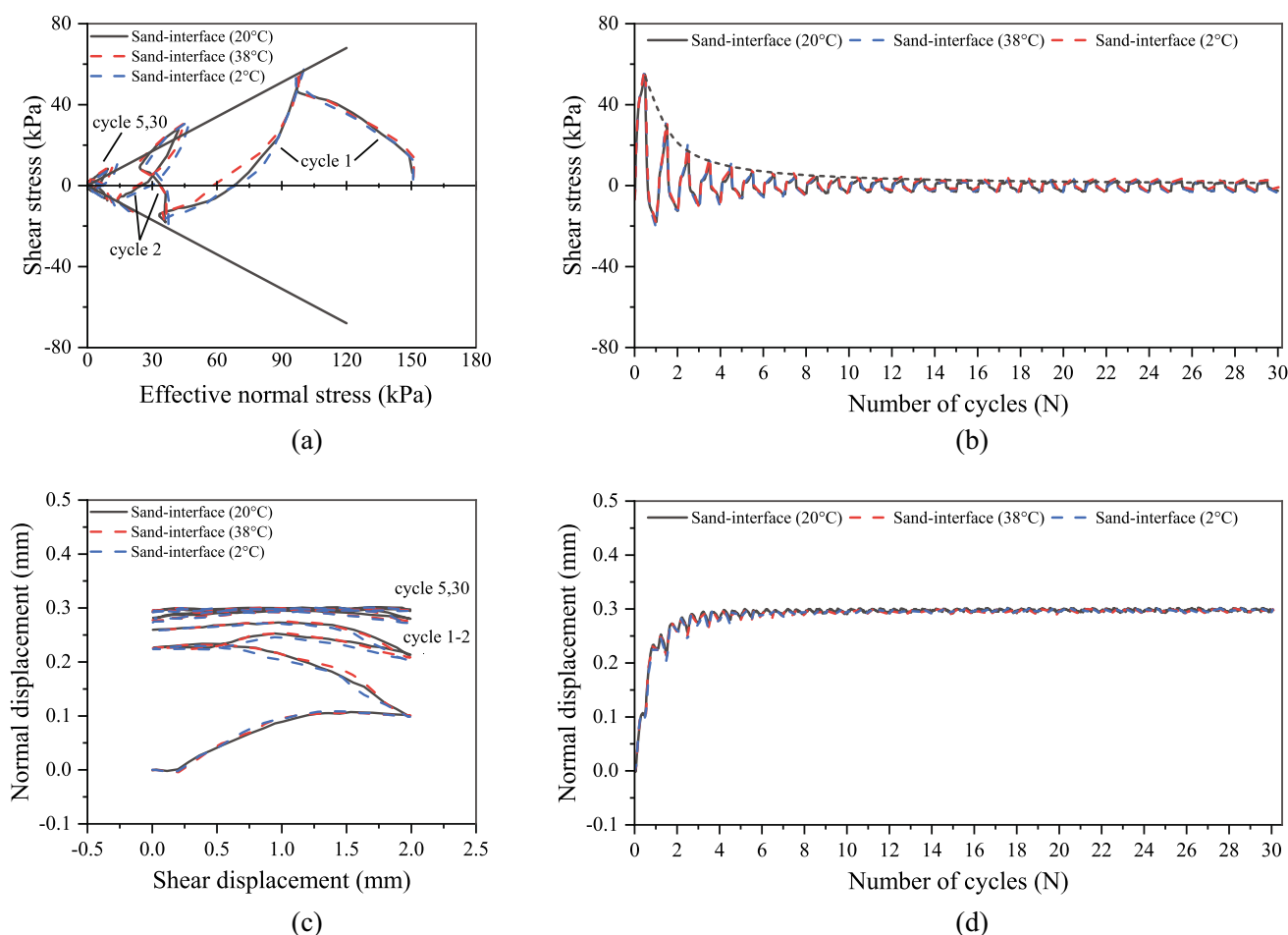


**Fig. 17** One-way cyclic shearing tests of sand–concrete interface at  $T = 2, 20, 38\text{ }^{\circ}\text{C}$  under CNS (500 kPa/mm) condition: **a** shear stress vs. displacement; **b** shear stress vs. cycle number; **c** normal displacement vs. shear displacement; **d** normal displacement vs. cycle number

(2) Thermal cycles could introduce volume reduction to the interface layer, depending on the soil type, stress level, and thermal load direction. For sand–concrete interfaces, both heating and cooling cycles introduced plastic deformation under lower normal stress, but elastic deformation under higher normal stress. For clay–concrete interfaces, heating cycles caused plastic deformation, while cooling cycles did not regardless of normal stress level, which is consistent with the observed thermal behaviour of clays.

(3) The volumetric strains caused by temperature variation have minimal influence on the volumetric response of specimens during monotonic shearing because of the insignificant strain magnitude (maximum 0.1% in monotonic thermal loading and maximum 0.23% in cyclic thermal loading).

(4) After heating cycles, the stress paths from CV shearing of clay–concrete interfaces exhibited a typical OC clay response during undrained shearing and therefore indicated that a lower excess pore pressure would be generated, and implying a potential to be characterised in

constitutive models with a temperature-dependent yield locus.

(5) The cyclic movements between the structure and surrounding soil, induced by annual or daily temperature variations (corresponding to two-way cyclic CNL shearing and one-way cyclic CNS shearing, respectively), are shown to likely cause more significant effects at the interface compared with the direct temperature effects. Such effects are more significant in CNS tests, where a medium-dense sand–concrete interface shear strength reached negligible values after 5 cycles, whereas a clay–concrete interface maintained 60% of its strength after 10 cycles.

(6) The cyclic shearing tests indicated the possible progressive reduction of shaft friction, especially for sand–concrete interfaces, and the consequences should be addressed in energy pile application. For piles founded in sand, which are generally considered end-bearing, this impact may not significantly reduce the bearing capacity, but it may result in changes in stress redistribution over cycles and additional settlements. In

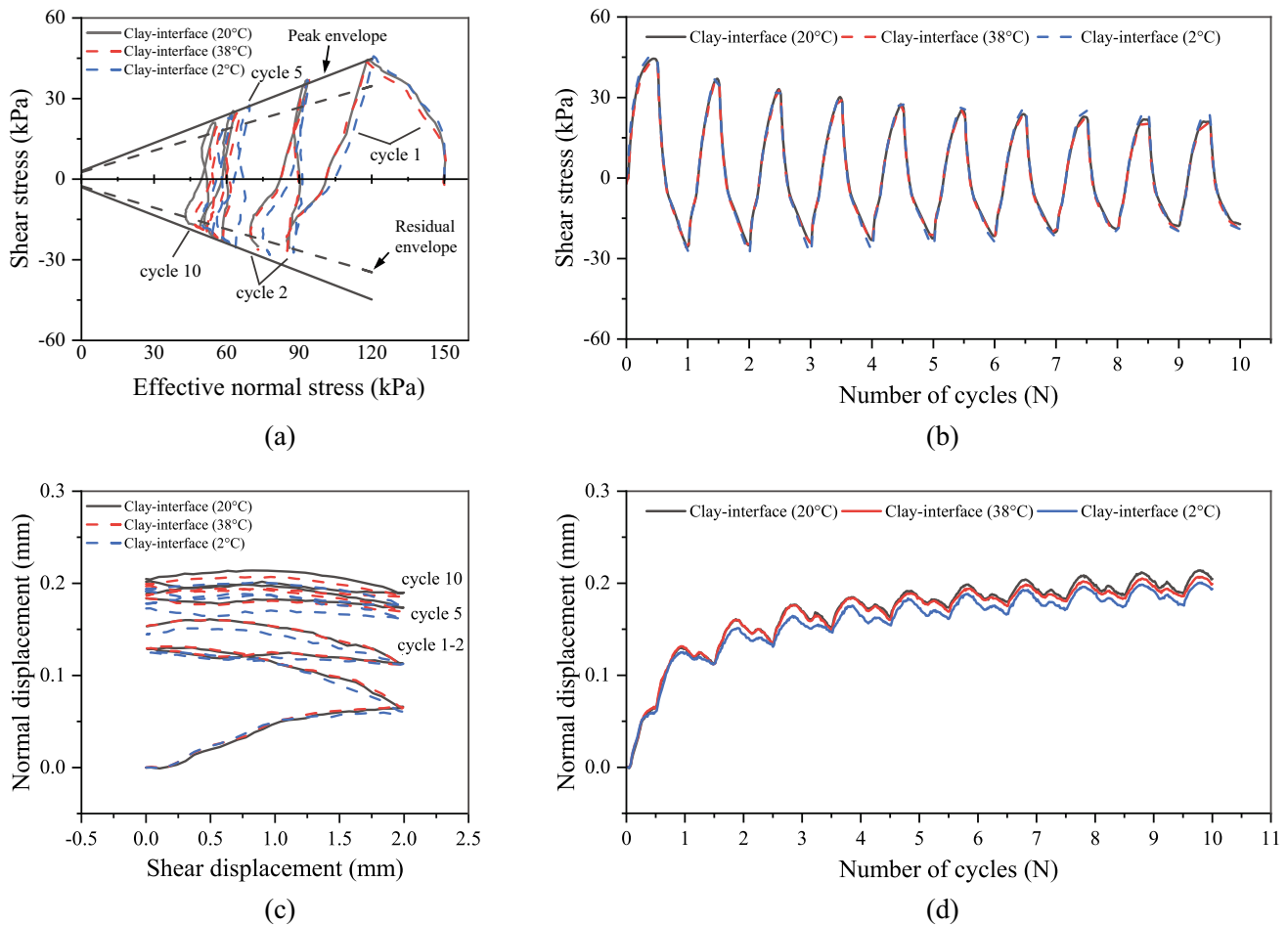


**Fig. 18** One-way cyclic shearing tests of clay–concrete interface at  $T = 2, 20, 38\text{ }^{\circ}\text{C}$  under CNS (500 kPa/mm) condition: **a** shear stress vs. displacement; **b** shear stress vs. cycle number; **c** normal displacement vs. shear displacement; **d** normal displacement vs. cycle number

floating piles, which rely on clay–concrete interface strength for both ultimate bearing capacity and settlements, this reduction in shear strength can be significant. However, for long-term loads (annual cycles), creep may increase the confining stresses and have a strengthening impact. The degree of such mechanical impacts will vary along the pile depending on the

relatively distance to the null point and magnitude of the temperature change.

## Appendix 1

See Table 2.

**Table 2** Summary of pre-sheared void ratio and volume change after shearing for Series I

Test	Material	Normal stress $\sigma_n$ (kPa)	Thermal path (°C)	$e_o$	$\Delta V_s$ (mm)
1	Sand	50	20	0.836	– 0.141
2		50	20–38	0.844	– 0.084
3		50	20–2	0.857	– 0.015
4		100	20	0.835	– 0.054
5		100	20–38	0.850	– 0.184
6		100	20–2	0.823	– 0.089
7		150	20	0.811	– 0.190
8		150	20–38	0.823	– 0.126
9		150	20–2	0.813	– 0.064
10	Sand–interface	50	20	0.839	0.128
11		50	20–38	0.821	0.071
12		50	20–2	0.839	0.156
13		100	20	0.823	0.105
14		100	20–38	0.837	0.218
15		100	20–2	0.821	0.056
16		150	20	0.824	0.166
17		150	20–38	0.826	0.162
18		150	20–2	0.826	0.158
19	Clay	50	20	1.015	0.129
20		50	20–38	1.055	0.166
21		50	20–2	1.058	0.186
22		100	20	0.979	0.192
23		100	20–38	1.037	0.345
24		100	20–2	1.017	0.307
25		150	20	0.984	0.361
26		150	20–38	0.977	0.395
27		150	20–2	0.979	0.291
28	Clay–concrete	50	20	1.063	0.212
29		50	20–38	1.047	0.137
30		50	20–2	1.022	0.103
31		150	20	0.967	0.179
32		150	20–38	0.962	0.177
33		150	20–2	0.945	0.212

$e_o$  = void ratio before temperature variation,  $\Delta V_s$  = volume change after shearing (+ for contraction, – or dilation)

## Appendix 2: Calibration of the temperature-controlled direct shear apparatus

The calibration of a modified direct shear apparatus manufactured by Wille Geotechnik in response to temperature change is presented here.

The shear box was kept in a climate room fixed at constant room temperature and was carefully insulated to

minimise thermal exchanges with the surroundings, although temperature changes are induced during the testing which had the potential to affect the sensor readings. In addition, consequential thermal expansion/contraction of the system may occur. Therefore, the system was calibrated for changes of temperature.

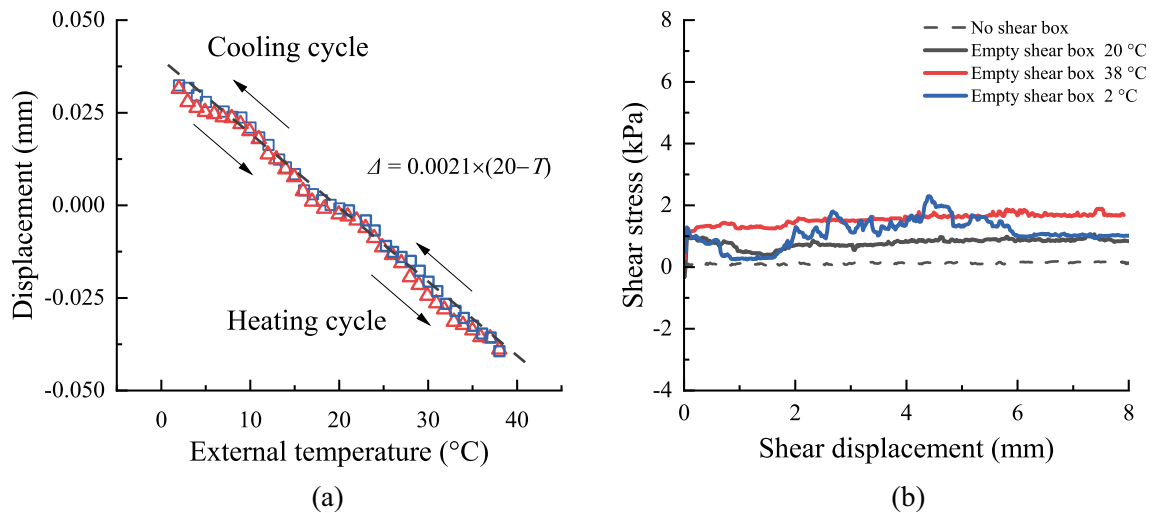


Fig. 19 Calibration of the apparatus: **a** vertical LVDT under thermal cycle; **b** shear stress under test temperature

### Calibration of the LVDT

The vertical displacements of samples subjected to mechanical and thermal loads are recorded via a vertical LVDT. An iron dummy sample (with known coefficient of thermal expansion) of 32 mm height was installed in the shear box, and a 50 kPa vertical stress was applied to ensure a full contact between the sample and the load cell. Subsequently, the sample was subjected to thermal cycles between 2 °C and 38 °C (covering the temperature range studied in this work) with a relatively slow rate of 5 °C/h, and displacements were recorded. The readings of the LVDT with the thermo-elastic deformations of the dummy sample subtracted, along with temperature variation, are shown in Fig. 19a. The recorded vertical displacement variation accounted for the thermal deformation from the components of the apparatus plus any temperature shift of the readings. The variation was seen to have an almost linear relationship with the temperature change and resulted in no apparent accumulation after thermal cycles. Therefore, all records from the vertical LVDT in this study were calibrated by a linear temperature calibration factor. For the horizontal LVDT, it changed by less than 0.002 mm during these thermal cycles, and thus, no calibration was necessary.

### Calibration of the shear stress

Two shear tests were conducted at ambient temperature (20 °C), with and without using the (empty) shear box, followed by two shear tests using the empty shear box at

2 °C and 38 °C. For the test without the shear box, the shear box was disassembled, and then, the shear test was conducted. The recorded shear stress accounted for the friction on the actuator motor. For the tests using the empty shear box, the load cap was lowered inside the shear box, filled with water, and insulated to minimise thermal losses. Then, after reaching the desired temperatures (with a thermal rate of 5 °C/h), shearing continued to 10 mm. The measured shear stresses against shear displacements are presented in Fig. 19b.

It is demonstrated that for the shear test without using the shear box (dashed line in Fig. 19b), the measured shear stress is negligible and remains almost constant (less than 0.05 kPa fluctuation) during the test. The test result with an empty shear box at ambient conditions yielded a mean shear stress of 0.90 kPa, which should be subtracted from the readings of the shear stress to extract the actual stress carried by the soil sample. For the shear tests with the empty shear box at 2 °C and 38 °C, it can be seen that the shear stress readings deviate by about 0.95 kPa and 1.73 kPa, respectively, from the test without the shear box. These values are subtracted from the measured shear stresses during data processing.

### Appendix 3: Examples of the primary consolidation

See Figure 20.

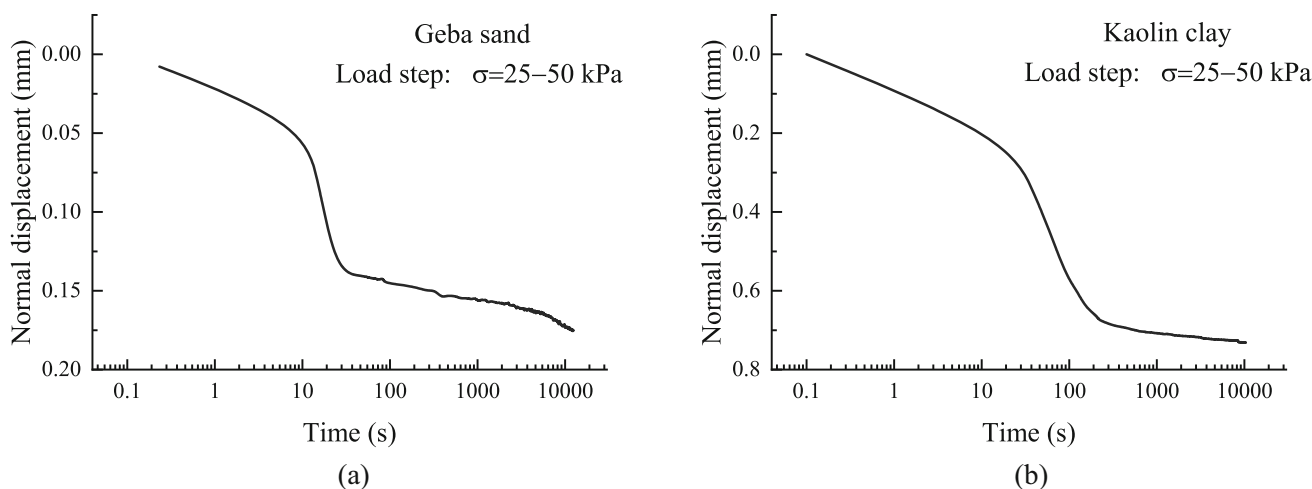


**Fig. 20** Examples of the primary consolidation process for the two soils: **a** Geba sand; **b** kaolin clay

**Acknowledgements** The authors would like to acknowledge the technical support from Wim Verwaal, Marc Friebel and Karel Heller for facilitating the experiments, incisive advice from Maghsoodi Soheib and detailed discussion and customisation of the operation software by Alborz Pourzargar (Wille Geotechnik). The authors would also like to thank Dr. Shuyang Zhang for providing the GSHP monitoring data. The first author was supported by the National Natural Science Foundation of China (Grant No. 41972269, No. 51778138), the Postgraduate Research & Practice Innovation Program of Jiangsu Province (Grant No. KYCX18\_0106) and the Chinese Scholarship Council. The work of the second, third and sixth authors was part of the research programme Energy Piles in the Netherlands with project number grant number 14698, financed by the Netherland Organisation for Scientific Research (NWO).

**Funding** National Natural Science Foundation of China, 41972269, Yimu Guo, 51778138, Yimu Guo, Postdoctoral Science Foundation of Jiangsu Province, KYCX18\_0106, Yimu Guo, China Scholarship Council, Nederlandse Organisatie voor Wetenschappelijk Onderzoek, 14698, Ali Golchin

**Data availability statement** The datasets generated during and/or analysed during the current study are available from the corresponding author on reasonable request.

## Declarations

**Conflict of interest** Michael Hicks is a member of the Acta Geotechnica editorial board and has not taken any part in handling or reviewing this paper. The authors declare that they have no other relevant financial or non-financial interests to disclose.

**Open Access** This article is licensed under a Creative Commons Attribution 4.0 International License, which permits use, sharing, adaptation, distribution and reproduction in any medium or format, as long as you give appropriate credit to the original author(s) and the source, provide a link to the Creative Commons licence, and indicate if changes were made. The images or other third party material in this article are included in the article's Creative Commons licence, unless indicated otherwise in a credit line to the material. If material is not included in the article's Creative Commons licence and your intended use is not permitted by statutory regulation or exceeds the permitted

use, you will need to obtain permission directly from the copyright holder. To view a copy of this licence, visit <http://creativecommons.org/licenses/by/4.0/>.

## References

- Brandl H (2006) Energy foundations and other thermo-active ground structures. *Géotechnique* 56(2):81–122
- Fang J, Kong G, Yang Q (2022) Group performance of energy piles under cyclic and variable thermal loading. *J Geotech Geoenviron Eng* 148(8):04022060
- Li R, Kong G, Chen Y, Yang Q (2021) Thermomechanical behaviour of an energy pile–raft foundation under intermittent cooling operation. *Geomech Energy Environ*. <https://doi.org/10.1016/j.gete.2021.100240>
- Hueckel T, Baldi G (1990) Thermoplasticity of saturated clays: experimental constitutive study. *J Geotech Eng* 116(12):1778–1796. [https://doi.org/10.1061/\(asce\)0733-9410\(1990\)116:12\(1778\)](https://doi.org/10.1061/(asce)0733-9410(1990)116:12(1778))
- Kuntiwattanakul P, Towhata I, Ohishi K, Seko I (1995) Temperature effects on undrained shear characteristics of clay. *Soils Found* 35(1):147–162
- Tanaka N, Graham J, Crilly T (1997) Stress-strain behaviour of reconstituted illitic clay at different temperatures. *Eng Geol* 47(4):339–350. [https://doi.org/10.1016/S0013-7952\(96\)00113-5](https://doi.org/10.1016/S0013-7952(96)00113-5)
- Burghignoli A, Desideri A, Miliziano S (2000) A laboratory study on the thermomechanical behaviour of clayey soils. *Can Geotech J* 37(4):764–780
- Marques MES, Leroueil S, de Almeida S, MdS, (2004) Viscous behaviour of St-Roch-de-l'Achigan clay. *Quebec Can Geotech J* 41(1):25–38. <https://doi.org/10.1139/t03-068>
- Cekerevac C, Laloui L (2004) Experimental study of thermal effects on the mechanical behaviour of a clay. *Int J Numer Anal Methods Geomech* 28(3):209–228. <https://doi.org/10.1002/nag.332>
- Abuel-Naga HM, Bergado DT, Lim BF (2007) Effect of temperature on shear strength and yielding behavior of soft Bangkok clay. *Soils Found* 47(3):423–436
- Alsherif NA, McCartney JS (2016) Yielding of silt at high temperature and suction magnitudes. *Geotech Geol Eng* 34(2):501–514

12. Yazdani S, Helwany S, Olgun G (2018) Experimental evaluation of shear strength of kaolin clay under cyclic and noncyclic thermal loading. *Geotech Test J* 42(6):20180020
13. Pastén C, Castillo E, Chong S-H (2019) Thermo-mechanical ratcheting in soil–structure interfaces. *Acta Geotech* 14(5):1561–1569. <https://doi.org/10.1007/s11440-019-00816-8>
14. Potyondy JG (1961) Skin friction between various soils and construction materials. *Géotechnique* 11(4):339–353
15. Yoshimi Y, Kishida T (1981) A ring torsion apparatus for evaluating friction between soil and metal surfaces. *Geotech Test J* 4(4):145–152
16. Uesugi M, Kishida H (1986) Frictional resistance at yield between dry sand and mild steel. *Soils Found* 26(4):139–149
17. Tehrani FS, Han F, Salgado R, Prezzi M, Tovar RD, Castro AG (2016) Effect of surface roughness on the shaft resistance of non-displacement piles embedded in sand. *Géotechnique* 66(5):386–400. <https://doi.org/10.1680/jgeot.15.P.007>
18. Martínez A, Frost JD (2017) The influence of surface roughness form on the strength of sand–structure interfaces. *Géotechnique Letters* 7(1):104–111. <https://doi.org/10.1680/jgele.16.00169>
19. Uesugi M, Kishida H, Uchikawa Y (1990) Friction between dry sand and concrete under monotonic and repeated loading. *Soils Found* 30(1):115–128
20. Paikowsky SG, Player CM, Connors PJ (1995) A dual interface apparatus for testing unrestricted friction of soil along solid surfaces. *Geotech Test J* 18(2):168–193
21. Martínez A, Frost JD, Hebel GL (2015) Experimental study of shear zones formed at sand/steel interfaces in axial and torsional axisymmetric tests. *Geotech Test J* 38(4):409–426
22. Afzali-Nejad A, Lashkari A, Shourijeh PT (2017) Influence of particle shape on the shear strength and dilation of sand-woven geotextile interfaces. *Geotext Geomembr* 45(1):54–66
23. Han F, Ganju E, Salgado R, Prezzi M (2018) Effects of interface roughness, particle geometry, and gradation on the sand–steel interface friction angle. *J Geotech Geoenviron Eng* 144(12):04018096
24. Lemos LJJ, Vaughan PR (2000) Clay–interface shear resistance. *Géotechnique* 50(1):55–64. <https://doi.org/10.1680/geot.2000.50.1.55>
25. Farhadi B, Lashkari A (2017) Influence of soil inherent anisotropy on behavior of crushed sand-steel interfaces. *Soils Found* 57(1):111–125. <https://doi.org/10.1016/j.sandf.2017.01.008>
26. Kishida H, Uesugi M (1987) Tests of the interface between sand and steel in the simple shear apparatus. *Géotechnique* 37(1):45–52. <https://doi.org/10.1680/geot.1987.37.1.45>
27. Tsubakihara Y, Kishida H (1993) Frictional behaviour between normally consolidated clay and steel by two direct shear type apparatuses. *Soils Found* 33(2):1–13
28. Taha A, Fall M (2012) Shear behavior of sensitive marine clay-concrete interfaces. *J Geotech Geoenviron Eng* 139(4):644–650
29. DeJong JT, Westgate ZJ (2009) Role of initial state, material properties, and confinement condition on local and global soil-structure interface behavior. *J Geotech Geoenviron Eng* 135(11):1646–1660. [https://doi.org/10.1061/\(ASCE\)1090-0241\(2009\)135:11\(1646\)](https://doi.org/10.1061/(ASCE)1090-0241(2009)135:11(1646))
30. Fakharian K, Evgin E (1997) Cyclic simple-shear behavior of sand-steel interfaces under constant normal stiffness condition. *J Geotech Geoenviron Eng* 123(12):1096–1105. [https://doi.org/10.1061/\(ASCE\)1090-0241\(1997\)123:12\(1096\)](https://doi.org/10.1061/(ASCE)1090-0241(1997)123:12(1096))
31. Porcino D, Fioravante V, Ghionna VN, Pedroni S (2003) Interface behavior of sands from constant normal stiffness direct shear tests. *Geotech Test J* 26(3):289–301
32. Johnston IW, Lam TSK, Williams AF (1987) Constant normal stiffness direct shear testing for socketed pile design in weak rock. *Géotechnique* 37(1):83–89. <https://doi.org/10.1680/geot.1987.37.1.83>
33. Fioravante V, Ghionna VN, Pedroni S, Porcino D (1999) A constant normal stiffness direct shear box for soil-solid interface tests. *Riv Italiana di Geotec* 33(3):7–22
34. Fioravante V (2002) On the shaft friction modelling of non-displacement piles in sand. *Soils Found* 42(2):23–33
35. Airey DW, Al-Douri RH, Poulos HG (1992) Estimation of pile friction degradation from shearbox tests. *Geotech Test J* 15(4):388–392
36. Tabucanon JT, Airey DW, Poulos HG (1995) Pile skin friction in sands from constant normal stiffness tests. *Geotech Test J* 18(3):350–364
37. Takada N (1993) Mikasa's direct shear apparatus, test procedures and results. *Geotech Test J* 16(3):314–322
38. Sadrekarimi A, Olson SM (2010) Shear band formation observed in ring shear tests on sandy soils. *J Geotech Geoenviron Eng* 136(2):366–375. [https://doi.org/10.1061/\(ASCE\)GT.1943-5606.0000220](https://doi.org/10.1061/(ASCE)GT.1943-5606.0000220)
39. Dyvik R, Berre T, Lacasse S, Raadim B (1987) Comparison of truly undrained and constant volume direct simple shear tests. *Géotechnique* 37(1):3–10. <https://doi.org/10.1680/geot.1987.37.1.3>
40. Kong G, Wu D, Liu H, Laloui L, Cheng X, Zhu X (2019) Performance of a geothermal energy deicing system for bridge deck using a pile heat exchanger. *Int J Energy Res* 43(1):596–603. <https://doi.org/10.1002/er.4266>
41. Di Donna A, Ferrari A, Laloui L (2015) Experimental investigations of the soil–concrete interface: physical mechanisms, cyclic mobilization, and behaviour at different temperatures. *Can Geotech J* 53(4):659–672
42. Wang DQ, Lu L, Cui P (2018) Simulation of thermo-mechanical performance of pile geothermal heat exchanger (PGHE) considering temperature-depend interface behavior. *Appl Therm Eng* 139:356–366. <https://doi.org/10.1016/j.applthermaleng.2018.02.020>
43. Vasilescu AR, Fauchille A-L, Dano C, Kotronis P, Manirakiza R, Gotteland P (2018) Impact of Temperature Cycles at Soil–Concrete Interface for Energy Piles. In: *International Symposium on Energy Geotechnics*: Springer p 35–42
44. Maghsoodi S, Cuisinier O, Masroufi F (2019) Thermal effects on the mechanical behaviour of the soil-structure interface. *Can Geotech J* 57(1):32–47. <https://doi.org/10.1139/cgj-2018-0583>
45. Yavari N, Tang AM, Pereira JM, Hassen G (2016) Effect of temperature on the shear strength of soils and the soil–structure interface. *Can Geotech J* 53(7):1186–1194. <https://doi.org/10.1139/cgj-2015-0355>
46. Li CH, Kong GQ, Liu HL, Abuel-Naga HM (2019) Effect of temperature on behaviour of red clay–structure interface. *Can Geotech J* 56(1):126–134. <https://doi.org/10.1139/cgj-2017-0310>
47. Ravera E, Sutman M, Laloui L (2021) Cyclic thermomechanical response of fine-grained soil–concrete interface for energy piles applications. *Can Geotech J* 58(8):1216–1230. <https://doi.org/10.1139/cgj-2020-0437>
48. Yazdani S, Helwany S, Olgun G (2019) Influence of temperature on soil-pile interface shear strength. *Geomech Energy Environ* 18:69–78. <https://doi.org/10.1016/j.gete.2018.08.001>
49. Maghsoudloo A, Askarnejad A, De Jager R, Molenkamp F, Hicks M (2018) Experimental investigation of pore pressure and acceleration development in static liquefaction induced failures in submerged slopes. In: *9th International Conference of Physical Modelling in Geotechnics*, London p 987–92
50. Zimnik AR, Van Baalen LR, Verhoef PN, Ngan-Tillard DJ (2000) The adherence of clay to steel surfaces. In: *ISRM International Symposium: International Society for Rock Mechanics and Rock Engineering*
51. BSI (1990) Part 2 Methods of test for soils for civil engineering purposes: classification tests. BSI, London, UK



52. ASTM (2011) D3080/D3080M-11 standard test method for direct shear test of soils under consolidated drained conditions. ASTM International, West Conshohocken, PA, USA
53. Hanzawa H, Nutt N, Lunne T, Tang YX, Long M (2007) A comparative study between the NGI direct simple shear apparatus and the Mikasa direct shear apparatus. *Soils Found* 47(1):47–58
54. Knellwolf C, Peron H, Laloui L (2011) Geotechnical analysis of heat exchanger piles. *J Geotech Geoenviron Eng* 137(10):890–902
55. Ng CWW, Wang SH, Zhou C (2016) Volume change behaviour of saturated sand under thermal cycles. *Géotech Lett* 6(2):124–131. <https://doi.org/10.1680/jgele.15.00148>
56. Uesugi M (1988) Behavior of sand particles in sand-steel friction. *Soils Found* 28(1):107
57. Vasilescu R, Yin K, Fauchille A-L, Kotronis P, Dano C, Manirakiza R, Gotteland P (2019) Influence of thermal cycles on the deformation of soil-pile interface in energy piles. *E3S Web Conf* 92:13004
58. Tsubakihara Y, Kishida H, Nishiyama T (1993) Friction between cohesive soils and steel. *Soils Found* 33(2):145–156. [https://doi.org/10.3208/sandf1972.33.2\\_145](https://doi.org/10.3208/sandf1972.33.2_145)
59. Parchment J, Shepley P (2018) The influence of temperature on shear strength at a soil-structure interface. In: *Proceedings of the 9th International Conference on Physical Modelling in Geotechnics (ICPMG 2018)*. CRC Press, London, UK. 149–53.
60. Bhushan B (2003) Adhesion and stiction: mechanisms, measurement techniques, and methods for reduction. *J Vac Sci Technol, B* 21(6):2262–2296
61. Golchin A, Vardon PJ, Hicks MA (2022) A thermo-mechanical constitutive model for fine-grained soils based on thermodynamics. *Int J Eng Sci* 174:103579. <https://doi.org/10.1016/j.ijengsci.2021.103579>
62. Lade PV, Liu CT (1998) Experimental study of drained creep behavior of sand. *J Eng Mech* 124(8):912–920
63. Mitchell JK, Soga K (2005) *Fundamentals of soil behavior* (3rd Edition). John Wiley & Sons, Hoboken, New Jersey
64. Laloui L, François B (2009) ACMEG-T: soil thermoplasticity model. *J Eng Mech* 135(9):932–944
65. Cui YJ, Sultan N, Delage P (2000) A thermomechanical model for saturated clays. *Can Geotech J* 37(3):607–620
66. Zhou C, Ng CWW (2015) A thermomechanical model for saturated soil at small and large strains. *Can Geotech J* 52(8):1101–1110. <https://doi.org/10.1139/cgj-2014-0229>
67. Radjai F, Jean M, Moreau JJ, Roux S (1996) Force distributions in dense two-dimensional granular systems. *Phys Rev Lett* 77(2):274
68. Sitharam TG (2003) Discrete element modelling of cyclic behaviour of granular materials. *Geotech Geol Eng* 21(4):297–329. <https://doi.org/10.1023/B:GEGE.0000006036.00597.0b>
69. Graham J, Tanaka N, Crilly T, Alfaro M (2001) Modified Cam-Clay modelling of temperature effects in clays. *Can Geotech J* 38(3):608–621
70. Perkins SW, Sjrursen M (2009) Effect of cold temperatures on properties of unfrozen troll clay. *Can Geotech J* 46(12):1473–1481
71. Trani L, Bergado D, Abuel-Naga HM (2013) Thermo-mechanical behavior of normally consolidated soft Bangkok clay. *Int J Geotech Eng* 4(1):31–44. <https://doi.org/10.3328/IJGE.2010.04.01.31-44>
72. Hueckel T, Pellegrini R (1992) Effective stress and water pressure in saturated clays during heating–cooling cycles. *Can Geotech J* 29(6):1095–1102
73. Laloui L, Cekerevac C (2003) Thermo-plasticity of clays: An isotropic yield mechanism. *Comput Geotech* 30(8):649–660
74. DeJong JT, White DJ, Randolph MF (2006) Microscale observation and modeling of soil-structure interface behavior using particle image velocimetry. *Soils Found* 46(1):15–28. <https://doi.org/10.3208/sandf.46.15>

**Publisher's Note** Springer Nature remains neutral with regard to jurisdictional claims in published maps and institutional affiliations.